Available online at www.sciencedirect.com
ScienceDirect
Journal of Sound and Vibration 298 (2006) 257–279
JOURNAL OF SOUND AND VIBRATION
www.elsevier.com/locate/jsvi

Coupled free vibrations of a cantilever plate with attached liquid drop

M. Chiba[a,*], T. Miyazawa[b], H. Baoyin[c]

[a]*Department of Aerospace Engineering, Graduate School of Engineering, Osaka Prefecture University, 1-1 Gakuen-cho, Naka-ku, Sakai 599-8531, Japan*
[b]*The Nippon Signal Co., Ltd., 3-1-1 Higashi-Ikebukuro, Tokyo 170-6047, Japan*
[c]*School of Aerospace, Tsinghua University, Beijing 100084, China*

Received 11 January 2006; received in revised form 8 May 2006; accepted 20 May 2006
Available online 31 July 2006

Abstract

Coupled free vibration analysis has been performed on a cantilever thin elastic plate carrying a liquid drop attached on its arbitrary point in a zero-gravity environment. A liquid drop, having slipping edge boundary condition on the plate, has been treated as an inviscid ideal liquid with hemi-spherical shape. By using Rayleigh–Ritz method, coupled hydroelastic problem has been rendered into an eigenvalue problem, from which one can obtain coupled natural frequencies and modes of vibration. Since we have treated an attached drop as an ideal liquid drop not as added rigid mass or 'mass–spring' system, the problem consists of coupled system between a plate and a liquid drop, which have both multi-degrees of freedom. In the numerical calculations, present results have been compared with the results in which a liquid drop have treated as a 'mass–spring' system which has previously been presented by the authors.

1. Introduction

Utilizing a low-gravity environment in space, a series of experiments, e.g. International Microgravity Laboratory (IML), United State Microgravity Laboratory (USML), First Microgravity Science Laboratory (MSL-1), etc., had been conducted in various fields of science such as material science, fundamental physics, life science, bioastronautics and so on. In material science, for example, new or high-quality materials, which cannot be produced on the ground, have been developed in space [1]. In such condition, heated liquefied material with free surface deforms to a spherical shape, minimizing its surface energy, and perfect spherical material with isotropic property can be obtained [2,3]. However, there are some problems which cannot be predicted on earth, i.e. Marangoni convection (vibration) [4], g-gitter [5], etc., which causes imperfection in shape or anisotropy of materials. Therefore, it may be a technical importance to clarify the vibrational behavior of a liquid drop itself or coupled dynamic behavior of a liquid drop with elastic supporting devices in low-gravity condition.

*Corresponding author. Tel./fax.: +81 72 254 9235.
E-mail address: chiba@aero.osakafu-u.ac.jp (M. Chiba).

0022-460X/$ - see front matter
doi:10.1016/j.jsv.2006.05.020

Nomenclature

a radius of liquid drop
D flexural rigidity of plate ($= Eh^3/12(1-\nu^2)$)
E Young's modulus of plate
h thickness of plate
H width of plate
L length of plate
$\tilde{L}$, $\tilde{\tilde{L}}$, $\bar{L}$, $\bar{\bar{L}}$ Lagrangian
m circumferential wavenumber
$P_n^m(\cos\theta)$ associated Legendre function
$r(\rho), \theta, \varphi$ spherical coordinate system (non-dimensional form)
$\mathbf{R}$ position vector
T kinetic energy
t (τ) time
U potential energy
V volume of liquid drop
$W(x,y,t)$ ($\bar{w}$) displacement of plate
$X_i(\xi)$ clamped–free beam function
$Y_j(\eta)$ free–free beam function
$x(\xi), y(\eta), z$ Cartesian coordinate system fixed at corner point of plate
$(x_0, y_0)(\xi_0, \eta_0)$ location of attached liquid drop
$Z(\theta,\varphi,t)$ ($\bar{\zeta}$) displacement of liquid–free surface
α plate thickness ratio ($= h/L$)
α_i characteristic values for clamped-free beam function
β drop radius ratio ($= h/a$)
β_j characteristic values for free–free beam function
δ surface tension parameter ($= \sigma h^2/D$)
$\bar{\Delta}$ parameter ($= \alpha^2\beta^2/\lambda\delta = DHh^2/\sigma a^2 L^3$)
ν Poisson's ratio of plate
λ aspect ratio ($= L/H$)
λ_{mn} zero of $\mathrm{d}P_n^m(\cos\theta)/\mathrm{d}\theta = 0$ at $\theta = \pi/2$
ρ_d density of liquid
ρ_p density of plate
$\bar{\rho}$ density ratio ($= \rho_p/\rho_d$)
σ surface tension
$\Phi(r,\theta,\varphi,t)$ velocity potential of liquid
$\mathbf{\Omega}$ rotational angular velocity vector
$\Omega(\omega)$ natural circular frequency ($\omega = \Omega/\Omega_p = \Omega/\sqrt{D/\rho_p h L^4}$)
Ω_p $= \sqrt{D/\rho_p h L^4}$
$\bar{\Omega}^2$ parameter ($= \Omega_p^2/\Omega_d^2 = D\rho_d a^3/\sigma\rho_p h L^4 = \alpha^4/\bar{\rho}\beta^3\delta$)

Taking up a coupled dynamic system in which liquid drop is added on a thin elastic structure from those above problems, we have simply modeled such system as a hemi-spherical liquid drop is added on a cantilever thin plate. And as a preliminary analysis, we have reduced added liquid drop to a simple 'spring–mass' system, i.e. to one-degree of freedom system [6], and clarified coupled natural frequencies and vibration modes by using *Rayleigh–Ritz* method, in which influence of an attached 'spring–mass' system, i.e. attached position, relative values of mass and spring constant, have been studied. Optimal position of an attached 'spring–mass' system to minimize coupled plate natural frequency has also been investigated.

As the next step, in the present paper, we shall treat added liquid drop as a frictionless ideal liquid drop of hemi-spherical shape, and clarify dynamic coupling characteristics with elastic plate by *Rayleigh–Ritz* method as has been used in Ref. [6]. When we look over the previous studies on liquid motions in a gravitational field, which have been treated from the energy method, in 1958, Miles proposed energy method for sloshing problem in a flexible tank [7]. In 1967, Luke applied variational principle to water wave problem [8] and Whitham analyzed nonlinear dispersion problem of water wave by using energy method [9]. Komatsu used Hamilton's principle to solved nonlinear sloshing problem of a liquid in an arbitrary shape tank [10]. As for a liquid drop problem, Natarajan and Brown [11,12] analyzed quadratic and third-order resonances of a liquid drop or bubble using modified Lagrangian which had been used by Luke [8] for free surface wave problem by replacing the gravitational energy with surface energy. Azuma and Yoshihara analyzed large-amplitude drop oscillations by using Lagrangian, which had been used in Refs. [11,12] and conducted experiment for mercury drops in drop tower [13].

While as for studies on vibrations of elastic plate with added sub-dynamical system, Das and Navaratna extended Young's study [14] which has been applied to a beam vibration with mass, spring and dashpot, to a simply supported rectangular plate at which one point is supported by a mass–spring system [15]. Snowdon studied forced vibration of a simply supported rectangular plate with an added mass or with a

mass–spring–dashpot system, and obtained force transmissibility and driving-point impedance of a plate [16]. Nicholson and Bergman extended their study [17] to a plate system [18]. Trentin and Guyader used modal sampling method to study response of a plate at medium frequency range in which a large number of modes exist [19]. Similar problem for a plate with mass–spring system was analyzed by Dowell and Tang by using asymptotic modal analysis [20]. Cha and Wong presented a method to analyze combined dynamical system and compared the results with those by Lagrange multiplier method, and Green function method [21]. In the optimization problem to maximize the fundamental natural frequency by adding support springs, Won and Park treated cantilever beam and plate [22]. Wu treated rectangular plate carrying multiple three-degree of freedom spring–mass system using equivalent mass method [23].

2. Free vibrations of a hemi-spherical drop on a rigid plane

First of all, we shall analyze free vibrations of a hemi-spherical drop alone on a rigid plane by using *Rayleigh–Ritz* method, as a preliminary examination of the application of the energy method to a plate-drop coupled dynamical system.

2.1. Analytical model

We shall consider small amplitude-free vibrations of a hemi-spherical drop of radius a on a rigid plane in a zero-gravity environment, as shown in Fig. 1. Spherical coordinate (r, θ, φ) with its origin o at the center of the drop base is used. Neglecting dynamics at the interface between liquid drop and base plane, e.g. contact angle, we here just take the kinematic condition between drop and base plane into account. Then there may be two types of contact conditions between drop and base, the one is slipping end condition (Fig. 1(a)) in which drop can move freely on the base, while the other is anchored end condition (Fig. 1(b)) in which drop sticks on the base along its circular boundary. In the present analysis, we shall employ the slipping condition: Fig. 1(a).

2.2. Basic equation

We assume that the liquid is incompressible, inviscid and behaves irrotational motion from which there exists velocity potential of the liquid $\Phi(r, \theta, \varphi, t)$, which satisfies *Laplace* equation

$$\Delta\Phi = \frac{\partial}{\partial r}\left(r^2 \frac{\partial \Phi}{\partial r}\right) + \frac{1}{\sin\theta}\frac{\partial}{\partial \theta}\left(\sin\theta \frac{\partial \Phi}{\partial \theta}\right) + \frac{1}{\sin^2\theta}\frac{\partial^2 \Phi}{\partial \varphi^2} = 0. \tag{1}$$

Kinetic energy T is given by

$$T = \frac{\rho_d}{2}\int_0^{2\pi}\int_0^{\pi/2}\int_0^{f(\theta,\varphi,t)} \{\nabla\Phi(r,\theta,\varphi,t)\cdot\nabla\Phi(r,\theta,\varphi,t)\} r^2 \sin\theta \, dr \, d\theta \, d\varphi, \tag{2}$$

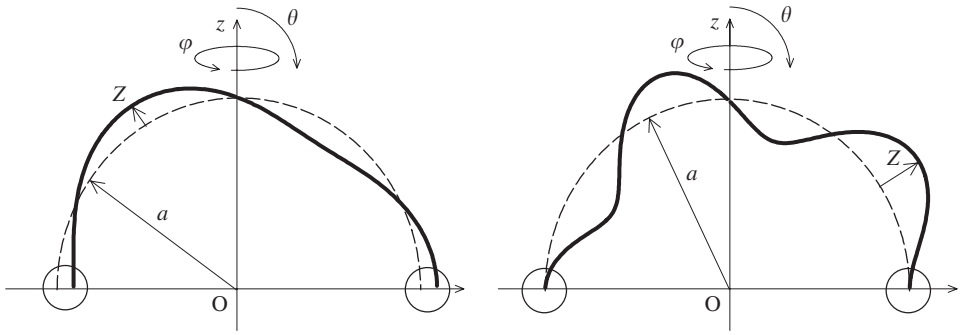

Fig. 1. Two types of contact conditions between semi-spherical drop and base.

where $f(\theta,\varphi,t)$ represents distances from origin to a free liquid surface:

$$f(\theta,\varphi,t)=a+Z(\theta,\varphi,t), \tag{3}$$

and $Z(\theta,\varphi,t)$ is free surface displacement, ρ_d is density of liquid. From the small amplitude assumption of the drop, one can obtain $f(\theta,\varphi,t)=a+Z(\theta,\varphi,t)\approx a$, and applying Green's theorem to Eq. (2),

$$T=\frac{\rho_d a^2}{2}\int_0^{2\pi}\int_0^{\pi/2}\left\{\Phi(r,\theta,\varphi,t)\frac{\partial\Phi(r,\theta,\varphi,t)}{\partial r}\right\}_{r=a}\sin\theta\,\mathrm{d}\theta\,\mathrm{d}\varphi. \tag{4}$$

While potential energy U due to the liquid surface tension σ is given by [11]

$$\begin{aligned}U=\sigma\int_0^{2\pi}\int_0^{\pi/2}f^2(\theta,\varphi,t)\left\{1+\frac{f_\theta^2(\theta,\varphi,t)}{f^2(\theta,\varphi,t)}+\frac{1}{\sin^2\theta}\frac{f_\varphi^2(\theta,\varphi,t)}{f^2(\theta,\varphi,t)}\right\}^{1/2}\sin\theta\,\mathrm{d}\theta\,\mathrm{d}\varphi\\ -\sigma\int_0^{2\pi}\int_0^{\pi/2}a^2\sin\theta\,\mathrm{d}\theta\,\mathrm{d}\varphi.\end{aligned} \tag{5}$$

Since

$$\frac{f_\theta^2(\theta,\varphi,t)}{f^2(\theta,\varphi,t)}+\frac{1}{\sin^2\theta}\frac{f_\varphi^2(\theta,\varphi,t)}{f^2(\theta,\varphi,t)}$$

may be small, putting

$$F(\theta,\varphi,t)=\frac{f_\theta^2(\theta,\varphi,t)}{f^2(\theta,\varphi,t)}+\frac{1}{\sin^2\theta}\frac{f_\varphi^2(\theta,\varphi,t)}{f^2(\theta,\varphi,t)}$$

and using Taylor expansions of $\{1+F(\theta,\varphi,t)\}^{1/2}$, we obtain

$$\sqrt{1+F(\theta,\varphi,t)}\approx 1+\frac{F(\theta,\varphi,t)}{2}. \tag{6}$$

Then Eq. (5) renders as

$$U=\sigma\int_0^{2\pi}\int_0^{\pi/2}\left[2aZ(\theta,\varphi,t)+Z^2(\theta,\varphi,t)+\frac{1}{2}\left\{Z_\theta^2(\theta,\varphi,t)+\frac{1}{\sin^2\theta}Z_\varphi^2(\theta,\varphi,t)\right\}\right]\sin\theta\,\mathrm{d}\theta\,\mathrm{d}\varphi. \tag{7}$$

Here from the assumption of the incompressibility of the drop, we obtain

$$\frac{1}{3}\int_0^{2\pi}\int_0^{\pi/2}\{a+Z(\theta,\varphi,t)\}^3\sin\theta\,\mathrm{d}\theta\,\mathrm{d}\varphi-V=0, \tag{8}$$

where $V(\equiv 2\pi a^3/3)$ is volume of the drop. Using Eqs. (7) and (8), we have

$$U=\sigma\int_0^{2\pi}\int_0^{\pi/2}\left[-Z^2(\theta,\varphi,t)+\frac{1}{2}\left\{Z_\theta^2(\theta,\varphi,t)+\frac{1}{\sin^2\theta}Z_\varphi^2(\theta,\varphi,t)\right\}\right]\sin\theta\,\mathrm{d}\theta\,\mathrm{d}\varphi. \tag{9}$$

Finally, we obtain *Lagrangian* $\tilde{L}$ of the system,

$$\begin{aligned}\tilde{L}&=T-U\\ &=\frac{\rho_d a^2}{2}\int_0^{2\pi}\int_0^{\pi/2}\left\{\Phi(r,\theta,\varphi,t)\frac{\partial\Phi(r,\theta,\varphi,t)}{\partial r}\right\}_{r=a}\sin\theta\,\mathrm{d}\theta\,\mathrm{d}\varphi\\ &\quad-\sigma\int_0^{2\pi}\int_0^{\pi/2}\left[-Z^2(\theta,\varphi,t)+\frac{1}{2}\left\{Z_\theta^2(\theta,\varphi,t)+\frac{1}{\sin^2\theta}Z_\varphi^2(\theta,\varphi,t)\right\}\right]\sin\theta\,\mathrm{d}\theta\,\mathrm{d}\varphi.\end{aligned} \tag{10}$$

Here, in order to represent free surface displacement of the drop $Z(\theta,\varphi,t)$ by means of the velocity potential $\Phi(r,\theta,\varphi,t)$, we use kinematic condition at the free surface.

$$\frac{\partial Z(\theta,\varphi,t)}{\partial t}=\frac{\partial\Phi(r,\theta,\varphi,t)}{\partial r}\ \text{at } r=a \text{ in the range } 0<\theta<\pi/2, \tag{11}$$

assuming $Z(\theta,\varphi,t)$ and $\Phi(r,\theta,\varphi,t)$ in the forms as

$$Z(\theta,\varphi,t)=\zeta(\theta,\varphi)\cos\ \Omega t,$$
$$\Phi(r,\theta,\varphi,t)=-\Omega\phi(r,\theta,\varphi)\sin\ \Omega t \tag{12}$$

and substituting into Eq. (11), we obtain the relation between $\zeta(\theta,\varphi)$ and $\phi(a,\theta,\varphi)$ as

$$\zeta(\theta,\varphi)=\frac{\partial\phi(a,\theta,\varphi)}{\partial r}. \tag{13}$$

Introducing Eq. (13) into Eq. (10), and integrating with t for one period of vibration, we obtain *Lagrangian* $\bar{L}=(\Omega/\pi)\tilde{L}$,

$$\bar{L}=\frac{\rho_d a^2\Omega^2}{2}\int_0^{2\pi}\int_0^{\pi/2}\left\{\phi(r,\theta,\varphi)\frac{\partial\phi(r,\theta,\varphi)}{\partial r}\right\}_{r=a}\sin\ \theta\,\mathrm{d}\theta\,\mathrm{d}\varphi$$
$$-\sigma\int_0^{2\pi}\int_0^{\pi/2}\left[-\left\{\frac{\partial\phi(r,\theta,\varphi)}{\partial r}\right\}^2+\frac{1}{2}\left\{\left\{\frac{\partial^2\phi(r,\theta,\varphi)}{\partial r\partial\theta}\right\}^2+\frac{1}{\sin^2\theta}\left\{\frac{\partial^2\phi(r,\theta,\varphi)}{\partial r\partial\varphi}\right\}^2\right\}\right]_{r=a}\sin\ \theta\,\mathrm{d}\theta\,\mathrm{d}\varphi. \tag{14}$$

2.3. Method of solution

The velocity potential $\phi(r,\theta,\varphi)$ is assumed to be of the form

$$\phi(r,\theta,\varphi)=\sum_{m=0}^{\infty}\sum_{n=0}^{\infty}A_{mn}\left(\frac{r}{a}\right)^{\lambda_{mn}}P^m_{\lambda_{mn}}(\cos\ \theta)\cos\ m\varphi, \tag{15}$$

where $P^m_{\lambda_{mn}}(\cos\ \theta)$ is the associated *Legendre* function of the first kind, and λ_{mn} are the roots of

$$\left.\frac{\mathrm{d}P^m_{\lambda_{mn}}(\cos\ \theta)}{\mathrm{d}\,\theta}\right|_{\theta=\pi/2}=0. \tag{16}$$

Substituting Eq. (15) into Eq. (14),

$$\bar{L}=\frac{\rho_d a\Omega^2\pi}{2}\sum_{m=0}^{\infty}\sum_{n=1}^{\infty}\sum_{s=1}^{\infty}A_{mn}A_{ms}\lambda_{ms}\int_0^{\pi/2}P^m_{\lambda_{mn}}(\cos\ \theta)P^m_{\lambda_{ms}}(\cos\ \theta)\sin\ \theta\,\mathrm{d}\,\theta$$
$$-\frac{\sigma\pi}{a^2}\left[-\sum_{m=0}^{\infty}\sum_{n=1}^{\infty}\sum_{s=1}^{\infty}A_{mn}A_{ms}\lambda_{mn}\lambda_{ms}\int_0^{\pi/2}P^m_{\lambda_{mn}}(\cos\ \theta)P^m_{\lambda_{ms}}(\cos\ \theta)\sin\ \theta\,\mathrm{d}\,\theta\right.$$
$$+\frac{1}{2}\sum_{m=0}^{\infty}\sum_{n=1}^{\infty}\sum_{s=1}^{\infty}A_{mn}A_{ms}\lambda_{mn}\lambda_{ms}\int_0^{\pi/2}\left\{\left(\frac{\partial}{\partial\theta}P^m_{\lambda_{mn}}(\cos\ \theta)\right)\left(\frac{\partial}{\partial\theta}P^m_{\lambda_{ms}}(\cos\ \theta)\right)\right.$$
$$\left.\left.+\frac{m^2}{\sin^2\theta}P^m_{\lambda_{mn}}(\cos\ \theta)P^m_{\lambda_{ms}}(\cos\ \theta)\right\}\sin\ \theta\,\mathrm{d}\,\theta\right], \tag{17}$$

and using following formulas of the associated *Legendre* function,

$$\int_0^{\pi/2}P^m_{\lambda_{mn}}(\cos\ \theta)P^m_{\lambda_{ms}}(\cos\ \theta)\mathrm{d}\,\theta=\frac{1}{2\lambda_{mn}+1}\cdot\frac{(\lambda_{mn}+m)!}{(\lambda_{mn}-m)!}\,\delta_{ns}, \tag{18}$$

$$\int_0^{\pi/2}\left\{\left(\frac{\partial P^m_{\lambda_{mn}}(\cos\ \theta)}{\partial\theta}\right)\left(\frac{\partial P^m_{\lambda_{ms}}(\cos\ \theta)}{\partial\theta}\right)+\frac{m^2}{\sin^2\theta}P^m_{\lambda_{mn}}(\cos\ \theta)P^m_{\lambda_{ms}}(\cos\ \theta)\right\}\sin\ \theta\,\mathrm{d}\,\theta$$
$$=\frac{\lambda_{mn}(\lambda_{mn}+1)}{2\lambda_{mn}+1}\cdot\frac{(\lambda_{mn}+m)!}{(\lambda_{mn}-m)!}\delta_{ns}. \tag{19}$$

We obtain

$$\overline{\bar{L}} = \sum_{m=0}^{\infty}\sum_{n=1}^{\infty} A_{mn}^2 \left\{ \Omega^2 - \frac{\sigma\lambda_{mn}}{\rho_d a^3}(\lambda_{mn}-1)(\lambda_{mn}+2) \right\} \frac{\lambda_{mn}}{2\lambda_{mn}+1} \cdot \frac{(\lambda_{mn}+m)!}{(\lambda_{mn}-m)!}, \tag{20}$$

where $\overline{\bar{L}} = 2\bar{L}/\rho_d a\pi$.

Then applying *Rayleigh–Ritz* method to the above equation,

$$\frac{\partial \bar{\bar{L}}}{\partial A_{mn}} = 0, \tag{21}$$

$$\frac{\partial \bar{\bar{L}}}{\partial A_{mn}} = \frac{\partial}{\partial A_{mn}} \left[\sum_{m=0}^{\infty}\sum_{n=1}^{\infty} A_{mn}^2 \left\{ \Omega^2 - \frac{\sigma\lambda_{mn}}{\rho_d a^3}(\lambda_{mn}-1)(\lambda_{mn}+2) \right\} \frac{\lambda_{mn}}{2\lambda_{mn}+1} \cdot \frac{(\lambda_{mn}+m)!}{(\lambda_{mn}+m)!} \right] = 0 \tag{22}$$

from which one can obtain

$$\left\{ \Omega^2 - \frac{\sigma\lambda_{mn}}{\rho_d a^3}(\lambda_{mn}-1)(\lambda_{mn}+2) \right\} A_{mn} = 0, \tag{23}$$

which renders,

$$\Omega^2 = \lambda_{mn}(\lambda_{mn}-1)(\lambda_{mn}+2)\frac{\sigma}{\rho_d a^3}. \tag{24}$$

This represents natural circular frequency of a hemi-spherical drop. Note that the Eq. (24) also represents natural frequency of a spherical drop [24]. Here, in the present case when $\theta = 90^\circ$, λ_{mn} are even numbers $2n$ for m is even, while these are odd numbers $2n-1$ for m is odd as

$$\begin{aligned} \Omega^2 &= 2n(2n-1)(2n+2)\frac{\sigma}{\rho_d a^3} \quad \text{for} \quad m = 2j, \\ &= (2n-1)(2n-2)(2n+1)\frac{\sigma}{\rho_d a^3} \quad \text{for} \quad m = 2j+1. \end{aligned} \tag{25}$$

So far we have obtained natural frequency of a hemi-spherical drop by using energy method, i.e. *Rayleigh–Ritz* method.

2.4. Numerical results

Natural circular frequencies of a semi-spherical drop $\Omega/\sqrt{\sigma/\rho_d a^3}$ calculated by Eq. (25) are presented in Table 1, and corresponding vibration modes are shown in Fig. 2 for up to the 4th mode with $m = 0, 1, 2$. $m = 0$ mode is an axisymmetric mode, while those with $m \neq 0$ are asymmetric modes. The first asymmetric vibration mode with $m = 1$ which has one nodal line along a meridian direction φ, has zero frequencies because of the slipping end conditions of the drop on the base here employed.

Table 1
Natural circular frequencies of a semi-spherical drop $\Omega/\sqrt{\sigma/\rho_d a^3}$

m	First	Second	Third	Fourth
0	2.8284271	8.4852814	15.491933	23.664319
1	0	5.4772256	11.832160	19.442222
2	2.8284271	8.4852814	15.491933	23.664319
3	5.4772256	11.832160	19.442222	28.142495

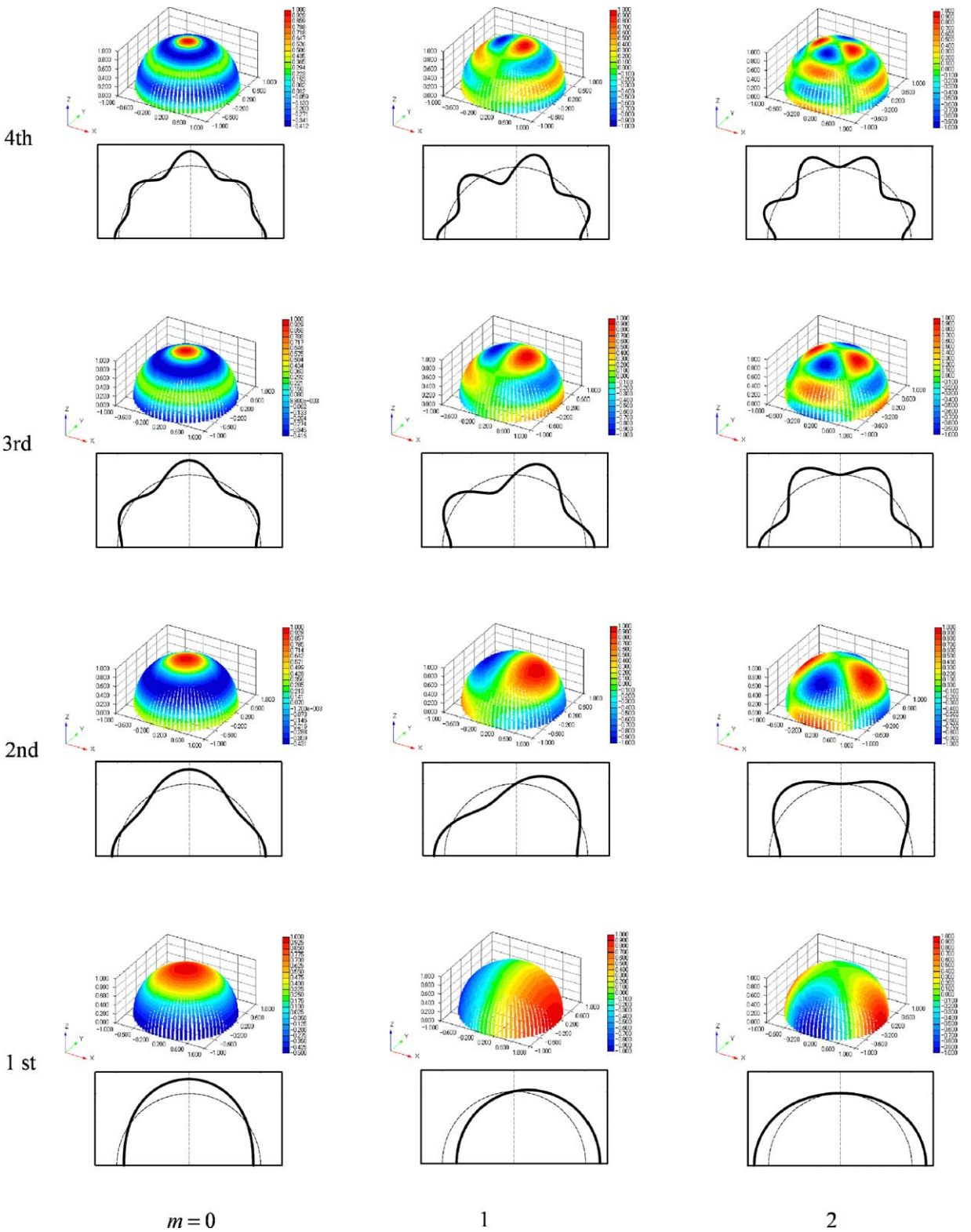

Fig. 2. Vibration modes of a semi-spherical drop on rigid plane.

3. Free vibrations of a plate-drop coupled system

3.1. Basic equation

Next, we shall consider coupled free vibrations of a thin cantilever plate attached by a liquid drop in a zero-gravity environment. Cartesian coordinate system $x-y-z$ is taken as shown in Fig. 3. The plate is thin and isotropic, with width H, length L, and thickness h. While the liquid drop attached at (x_0, y_0) on the plate, is incompressible, inviscid liquid and behaves irrotational motion. The static shape of the drop is assumed to be hemi-sphere with radius $r = a$, which is smaller than length L, and width H of the plate. The boundary condition of the drop on the plate is the slipping edge condition as described in the previous chapter (see Fig. 1(a)). Here, we shall use (o, x, y, z) coordinate system for the plate, while for the drop we shall use (o, r, θ, φ) coordinate system whose origin is fixed at point (x_0, y_0) on the plate. Displacements of the plate and the free surface of the drop are represented as $W(x, y, t)$ and $Z(\theta, \varphi, t)$, respectively.

The velocity of the drop can be represented by the velocity potential $\Phi(r, \theta, \varphi, t)$ which satisfies the *Laplace* equation,

$$\Delta\Phi(r,\theta,\varphi,t) = \frac{\partial}{\partial r}\left(r^2\frac{\partial\Phi(r,\theta,\varphi,t)}{\partial r}\right) + \frac{1}{\sin\theta}\frac{\partial}{\partial\theta}\left(\sin\theta\frac{\partial\Phi(r,\theta,\varphi,t)}{\partial\theta}\right) + \frac{1}{\sin^2\theta}\frac{\partial^2\Phi(r,\theta,\varphi,t)}{\partial\varphi^2} = 0. \tag{26}$$

Kinetic energy T and potential energy U of the system are

$$\begin{aligned} T = {} & \frac{\rho_p h}{2}\int_0^H\int_0^L \dot{W}^2(x,y,t)\,\mathrm{d}x\,\mathrm{d}y \\ & + \frac{\rho_d}{2}\int_0^{2\pi}\int_0^{\pi/2}\int_0^a \left\{\dot{W}(x_0,y_0,t) + \boldsymbol{\Omega}\times\mathbf{R} + \nabla\Phi(r,\theta,\varphi,t)\right\} \\ & \times\left\{\dot{W}(x_0,y_0,t) + \boldsymbol{\Omega}\times\mathbf{R} + \nabla\Phi(r,\theta,\varphi,t)\right\} r^2\sin\theta\,\mathrm{d}r\,\mathrm{d}\theta\,\mathrm{d}\varphi, \end{aligned} \tag{27}$$

$$\begin{aligned} U = {} & \frac{D}{2}\int_0^H\int_0^L \left[\left(\frac{\partial^2 W(x,y,t)}{\partial x^2}\right)^2 + \left(\frac{\partial^2 W(x,y,t)}{\partial y^2}\right)^2\right. \\ & \left. + 2\nu\frac{\partial^2 W(x,y,t)}{\partial x^2}\frac{\partial^2 W(x,y,t)}{\partial y^2} + 2(1-\nu)\left(\frac{\partial^2 W(x,y,t)}{\partial x\partial y}\right)^2\right]\mathrm{d}x\,\mathrm{d}y \\ & + \sigma\int_0^{2\pi}\int_0^{\pi/2}\left[-Z^2(\theta,\varphi,t) + \frac{1}{2}\left\{Z_\theta^2(\theta,\varphi,t) + \frac{1}{\sin^2\theta}Z_\varphi^2(\theta,\varphi,t)\right\}\right]\sin\theta\,\mathrm{d}\theta\,\mathrm{d}\varphi. \end{aligned} \tag{28}$$

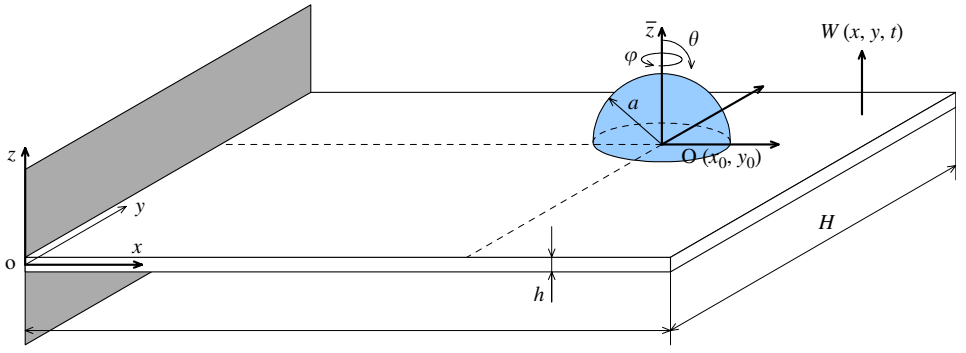

Fig. 3. Cantilever plate attached with semi-spherical drop.

In the above equations, $\mathbf{\Omega} \times \mathbf{R}$ represents an effect of rotational motion of the drop, ρ_p is the density and D is the flexural rigidity of the plate. Then we can obtain *Lagrangian* $\bar{\bar{L}}$ as

$$\begin{aligned}
\bar{\bar{L}} &= T - U \\
&= \frac{\rho_p h}{2}\int_0^H\int_0^L \dot{W}^2(x,y,t)\,\mathrm{d}x\,\mathrm{d}y \\
&\quad + \frac{\rho_d}{2}\int_0^{2\pi}\int_0^{\pi/2}\int_0^a \left\{\dot{W}(x_0,y_0,t) + \mathbf{\Omega}\times\mathbf{R} + \nabla\Phi(r,\theta,\varphi,t)\right\} \\
&\quad \times\left\{\dot{W}(x_0,y_0,t) + \mathbf{\Omega}\times\mathbf{R} + \nabla\Phi(r,\theta,\varphi,t)\right\} r^2\,\sin\,\theta\,\mathrm{d}r\,\mathrm{d}\theta\,\mathrm{d}\varphi \\
&\quad - \frac{D}{2}\int_0^H\int_0^L\left[\left(\frac{\partial^2 W(x,y,t)}{\partial x^2}\right)^2 + \left(\frac{\partial^2 W(x,y,t)}{\partial y^2}\right)^2\right. \\
&\quad \left. + 2\nu\frac{\partial^2 W(x,y,t)}{\partial x^2}\frac{\partial^2 W(x,y,t)}{\partial y^2} + 2(1-\nu)\left(\frac{\partial^2 W(x,y,t)}{\partial x\partial y}\right)^2\right]\mathrm{d}x\,\mathrm{d}y \\
&\quad - \sigma\int_0^{2\pi}\int_0^{\pi/2}\left[-Z^2(\theta,\varphi,t) + \frac{1}{2}\left\{Z_\theta^2(\theta,\varphi,t) + \frac{1}{\sin^2\theta}Z_\varphi^2(\theta,\varphi,t)\right\}\right]\sin\,\theta\,\mathrm{d}\theta\,\mathrm{d}\varphi.
\end{aligned} \tag{29}$$

In the analysis hereafter, we shall assume that the drop behaves just vertical motion with small amplitude on the plate ignoring the rotational motion, i.e. $\mathbf{\Omega}\times\mathbf{R} = 0$, which can be realized when a drop is attached on a loop of vibration mode of the plate. Here introducing the following non-dimensional parameters, the above-obtained equations are non-dimensionalized with $\bar{L} = 2\bar{\bar{L}}\Big/\sigma a^2$,

$$\begin{aligned}
&\xi = \frac{x}{L}, \quad \eta = \frac{y}{H}, \quad \bar{w} = \frac{W}{h}, \quad \tau = \Omega_p t, \quad \Omega_d = \sqrt{\frac{\sigma}{\rho_d a^3}}, \\
&\alpha = \frac{h}{L}, \quad \lambda = \frac{L}{H}, \quad \xi_0 = \frac{x_0}{L}, \quad \eta_0 = \frac{y_0}{H}, \quad \bar{w} = \frac{W}{h}, \\
&\rho = \frac{r}{a}, \quad \bar{\phi} = \frac{\Phi}{\Omega_p a^2}, \quad \bar{\zeta} = \frac{Z}{a}, \quad \beta = \frac{h}{a}, \quad \Omega_p = \sqrt{\frac{D}{\rho_p h L^4}}, \\
&\bar{\Omega} = \frac{\Omega_p}{\Omega_d} = \sqrt{\frac{\alpha^4}{\beta^3\bar{\rho}\delta}}, \quad \delta = \frac{\sigma h^2}{D}, \quad \bar{\Delta} = \frac{\alpha^2\beta^2}{\lambda\delta}, \quad \bar{\rho} = \frac{\rho_p}{\rho_d},
\end{aligned} \tag{30}$$

where λ is the aspect ratio of the plate, α is non-dimensional thickness of the plate, β is radius ratio, $\bar{\rho}$ is density ratio, δ is surface tension parameter. With parameters λ and α, plate dimension is defined, and with β drop dimension is determined. While $\bar{\rho}$ and δ are the parameters, which characterize material property. These parameters represent the present coupled vibration system together with attached position of the drop (ξ_0, η_0).

$$\begin{aligned}
\bar{L} &= \bar{\Delta}\int_0^1\int_0^1\left(\frac{\partial\bar{w}(\xi,\eta,\tau)}{\partial\tau}\right)^2\mathrm{d}\xi\,\mathrm{d}\eta \\
&\quad - \bar{\Delta}\int_0^1\int_0^1\left[\left(\frac{\partial^2\bar{w}(\xi,\eta,\tau)}{\partial\xi^2}\right)^2 + \lambda^4\left(\frac{\partial^2\bar{w}(\xi,\eta,\tau)}{\partial\eta^2}\right)^2 + 2\nu\lambda^2\frac{\partial^2\bar{w}(\xi,\eta,\tau)}{\partial\xi^2}\frac{\partial^2\bar{w}(\xi,\eta,\tau)}{\partial\eta^2}\right. \\
&\quad \left. + 2(1-\nu)\lambda^2\left(\frac{\partial^2\bar{w}(\xi,\eta,\tau)}{\partial\xi\partial\eta}\right)^2\right]\mathrm{d}\xi\,\mathrm{d}\eta \\
&\quad + \bar{\Omega}^2\int_0^{2\pi}\int_0^{\pi/2}\int_0^1\left[\beta^2\left(\frac{\partial\bar{w}(\xi_0,\eta_0,\tau)}{\partial\tau}\right)^2 + 2\beta\frac{\partial\bar{w}(\xi_0,\eta_0,\tau)}{\partial\tau}\left\{\frac{\partial\bar{\phi}(\rho,\theta,\varphi,\tau)}{\partial\rho} + \frac{1}{\rho}\frac{\partial\bar{\phi}(\rho,\theta,\varphi,\tau)}{\partial\theta}\right.\right. \\
&\quad \left.\left. + \frac{1}{\rho\,\sin\,\theta}\frac{\partial\bar{\phi}(\rho,\theta,\varphi,\tau)}{\partial\varphi}\right\}\right]\rho^2\,\sin\,\theta\,\mathrm{d}\rho\,\mathrm{d}\theta\,\mathrm{d}\varphi
\end{aligned}$$

$$+\bar{\Omega}^2\int_0^{2\pi}\int_0^{\pi/2}\left\{\bar{\phi}(\rho,\theta,\varphi,\tau)\frac{\partial\bar{\phi}(\rho,\theta,\varphi,\tau)}{\partial\rho}\right\}_{\rho=1}\sin\theta\,\mathrm{d}\theta\,\mathrm{d}\varphi$$
$$-2\int_0^{2\pi}\int_0^{\pi/2}\left[-\bar{\zeta}^2(\theta,\varphi,\tau)+\frac{1}{2}\left\{\bar{\zeta}_\theta^2(\theta,\varphi,\tau)+\frac{1}{\sin^2\theta}\bar{\zeta}_\varphi^2(\theta,\varphi,\tau)\right\}\right]\sin\theta\,\mathrm{d}\theta\,\mathrm{d}\varphi. \tag{31}$$

In order to represent free surface displacement of the drop $\bar{\zeta}(\theta,\varphi,\tau)$ by means of the velocity potential $\bar{\phi}(\rho,\theta,\varphi,\tau)$, we use kinematic condition at the free surface.

$$\frac{\partial\bar{\zeta}(\theta,\varphi,\tau)}{\partial\tau}=\frac{\partial\bar{\phi}(\rho,\theta,\varphi,\tau)}{\partial\rho}\quad\text{at }\rho=1\quad\text{in the range }0<\theta<\pi/2. \tag{32}$$

Here, $\bar{\zeta}(\theta,\varphi,\tau)$, $\bar{\phi}(\rho,\theta,\varphi,\tau)$ and $\bar{w}(\xi,\eta,\tau)$ are assumed in the forms as

$$\begin{aligned}\bar{\zeta}(\theta,\varphi,t)&=\zeta(\theta,\varphi)\cos\omega\tau,\\ \bar{\phi}(\rho,\theta,\varphi,\tau)&=-\omega\phi(\rho,\theta,\varphi)\sin\omega\tau,\\ \bar{w}(\xi,\eta,\tau)&=w(\xi,\eta)\cos\omega\tau,\end{aligned} \tag{33}$$

where ω is non-dimensional coupled natural frequency defined as

$$\omega=\frac{\Omega}{\Omega_p},\quad \Omega_p=\sqrt{\frac{D}{\rho_p hL^4}}. \tag{34}$$

With Eqs. (32) and (33), we obtain the relation between $\zeta(\theta,\varphi)$ and $\phi(\rho,\theta,\varphi)$ as

$$\zeta(\theta,\varphi)=\left.\frac{\partial\phi(\rho,\theta,\varphi)}{\partial\rho}\right|_{\rho=1}. \tag{35}$$

Substituting Eqs. (33) and (35) into Eq. (31), and integrating with t, we obtain *Lagrangian* $\tilde{\tilde{L}}$ for the coupled dynamic system between plate and drop.

$$\begin{aligned}\tilde{\tilde{L}}=\bar{\Delta}\omega^2&\int_0^1\int_0^1 w^2(\xi,\eta)\mathrm{d}\xi\,\mathrm{d}\eta\\
&-\bar{\Delta}\int_0^1\int_0^1\left[\left(\frac{\partial^2 w(\xi,\eta)}{\partial\xi^2}\right)^2+\lambda^4\left(\frac{\partial^2 w(\xi,\eta)}{\partial\eta^2}\right)^2\right.\\
&\left.+2\nu\lambda^2\frac{\partial^2 w(\xi,\eta)}{\partial\xi^2}\frac{\partial^2 w(\xi,\eta)}{\partial\eta^2}+2(1-\nu)\lambda^2\left(\frac{\partial^2 w(\xi,\eta)}{\partial\xi\partial\eta}\right)^2\right]\mathrm{d}\xi\,\mathrm{d}\eta\\
&+\bar{\Omega}^2\omega^2\int_0^{2\pi}\int_0^{\pi/2}\int_0^1\left[\beta^2 w^2(\xi_0,\eta_0)+2\beta w(\xi_0,\eta_0)\right.\\
&\left.\times\left\{\frac{\partial\phi(\rho,\theta,\varphi)}{\partial\rho}+\frac{1}{\rho}\frac{\partial\phi(\rho,\theta,\varphi)}{\partial\theta}+\frac{1}{\rho\sin\theta}\frac{\partial\phi(\rho,\theta,\varphi)}{d\varphi}\right\}\right]\rho^2\sin\theta\,\mathrm{d}\rho\,\mathrm{d}\theta\,\mathrm{d}\varphi\\
&+\bar{\Omega}^2\omega^2\int_0^{2\pi}\int_0^{\pi/2}\left\{\phi(\rho,\theta,\varphi,\tau)\frac{\partial\phi(\rho,\theta,\varphi,\tau)}{\partial\rho}\right\}_{\rho=1}\sin\theta\,\mathrm{d}\theta\,\mathrm{d}\varphi\\
&-2\int_0^{2\pi}\int_0^{\pi/2}\left[-\left\{\frac{\partial\phi(\rho,\theta,\varphi)}{\partial\rho}\right\}^2\right.\\
&\left.+\frac{1}{2}\left\{\left\{\frac{\partial\phi(\rho,\theta,\varphi)}{\partial\rho\partial\theta}\right\}^2+\frac{1}{\sin^2\theta}\left\{\frac{\partial\phi(\rho,\theta,\varphi)}{\partial\rho\partial\varphi}\right\}^2\right\}\right]_{\rho=1}\sin\theta\,\mathrm{d}\,\theta\,\mathrm{d}\varphi.\end{aligned} \tag{36}$$

3.2. Method of solution

We will apply *Rayleigh–Ritz* method to Eq. (36). The deflection of the plate $w(\xi,\eta)$ and the velocity potential of the drop $\phi(\rho,\theta,\varphi)$ are assumed to be of the forms:

$$w(\xi,\eta)=\sum_{i=1}^{\infty}\sum_{j=1}^{\infty}A_{ij}X_i(\xi)Y_j(\eta), \tag{37}$$

$$\phi(\rho,\theta,\varphi)=\sum_{m=0}^{\infty}\sum_{n=1}^{\infty}B_{mn}\rho^{\lambda_{mn}}P^m_{\lambda_{mn}}(\cos\theta)\cos m\varphi, \tag{38}$$

where A_{ij} and B_{mn} are the unknown coefficients. $X_i(\xi)$ and $Y_j(\eta)$ are admissible beam functions which satisfy *clamped–free* boundary conditions and *free–free* conditions, respectively, which are defined as follows [25]:

$$X_i(\xi)=\mu_i(\cosh\alpha_i\xi-\cos\alpha_i\xi)-v_i(\sinh\alpha_i\xi-\sin\alpha_i\xi),\quad (0<\xi<1,\quad i=1,2,3,\ldots) \tag{39}$$

$$\mu_i=\frac{\cosh\alpha_i+\cos\alpha_i}{\sinh\alpha_i\cdot\sin\alpha_i},\quad v_i=\frac{\sinh\alpha_i-\sin\alpha_i}{\sinh\alpha_i\cdot\sin\alpha_i}, \tag{40}$$

where α_i are the roots of

$$\cosh\alpha_i\cdot\cos\alpha_i=-1, \tag{41}$$

$\alpha_1=1.875,\quad \alpha_2=4.694,\quad \alpha_3=7.854,\ldots$ for *clamped–free* beam function:

$$\begin{aligned}&Y_1(\eta)=1,\\&Y_2(\eta)=\sqrt{3}(2\eta-1),\\&Y_j(\eta)=\bar{\mu}_j(\cosh\beta_j\eta+\cos\beta_j\eta)-\bar{v}_j(\sinh\beta_j\eta+\sin\beta_j\eta)\\&\qquad(0<\eta<1,\quad j=3,4,5,\ldots),\end{aligned} \tag{42}$$

$$\bar{\mu}_j=\frac{\cosh\beta_j-\cos\beta_j}{\sinh\beta_j\cdot\sin\beta_j},\quad \bar{v}_j=\frac{\sinh\beta_j+\sin\beta_j}{\sinh\beta_j\cdot\sin\beta_j}, \tag{43}$$

where $\beta_j(3\leqslant j)$ are the roots of

$$\cosh\beta_j\cdot\cos\beta_j=1, \tag{44}$$

$\beta_3=4.730,\quad \beta_4=7.853,\quad \beta_5=10.995,\ldots$ for *free–free* beam function.

While $P^m_{\lambda_{mn}}(\cos\theta)$ is the associated *Legendre* function of the first kind, and λ_{mn} are the roots of

$$\left.\frac{\mathrm{d}P^m_{\lambda_{mn}}(\cos\theta)}{\mathrm{d}\theta}\right|_{\theta=\pi/2}=0. \tag{45}$$

Substituting Eqs. (37) and (38) into Eq. (36),

$$\begin{aligned}\tilde{\tilde{L}}=&\bar{\Delta}\omega^2\sum_{i=1}^{\infty}\sum_{j=1}^{\infty}\sum_{k=1}^{\infty}\sum_{l=1}^{\infty}A_{ij}A_{kl}\int_0^1X_i(\xi)X_k(\xi)\,\mathrm{d}\xi\int_0^1Y_j(\eta)Y_l(\eta)\,\mathrm{d}\eta\\&-\bar{\Delta}\sum_{i=1}^{\infty}\sum_{j=1}^{\infty}\sum_{k=1}^{\infty}\sum_{l=1}^{\infty}A_{ij}A_{kl}\left[\int_0^1\frac{\mathrm{d}^2X_i(\xi)}{\mathrm{d}\xi^2}\frac{\mathrm{d}^2X_k(\xi)}{\mathrm{d}\xi^2}\,\mathrm{d}\xi\int_0^1Y_j(\eta)Y_l(\eta)\,\mathrm{d}\eta\right.\end{aligned}$$

$$+\lambda^4\int_0^1 X_i(\xi)X_k(\xi)\,\mathrm{d}\xi\int_0^1\frac{\mathrm{d}^2Y_j(\eta)}{\mathrm{d}\eta^2}\frac{\mathrm{d}^2Y_l(\eta)}{\mathrm{d}\eta^2}\,\mathrm{d}\eta+\nu\lambda^2\left\{\int_0^1\frac{\mathrm{d}^2X_i(\xi)}{\mathrm{d}\xi^2}X_k(\xi)\,\mathrm{d}\xi\int_0^1 Y_j(\eta)\frac{\mathrm{d}^2Y_l(\eta)}{\mathrm{d}\eta^2}\,\mathrm{d}\eta\right.$$
$$\left.+\int_0^1 X_i(\xi)\frac{\mathrm{d}^2X_k(\xi)}{\mathrm{d}\xi^2}\mathrm{d}\xi\int_0^1\frac{\mathrm{d}^2Y_j(\eta)}{\mathrm{d}\eta^2}Y_l(\eta)\,\mathrm{d}\eta\right\}+2(1-\nu)\lambda^2\int_0^1\frac{\mathrm{d}X_i(\xi)}{\mathrm{d}\xi}\frac{\mathrm{d}X_k(\xi)}{\mathrm{d}\xi}\,\mathrm{d}\xi\int_0^1\frac{\mathrm{d}Y_j(\eta)}{\mathrm{d}\eta}\frac{\mathrm{d}Y_l(\eta)}{\mathrm{d}\eta}\,\mathrm{d}\eta\Bigg]$$
$$+\bar{\Omega}^2\omega^2\left[\beta^2\sum_{i=1}^{\infty}\sum_{j=1}^{\infty}\sum_{k=1}^{\infty}\sum_{l=1}^{\infty}A_{ij}A_{kl}X_i(\xi_0)X_k(\xi_0)Y_j(\eta_0)Y_l(\eta_0)\int_0^{2\pi}\int_0^{\pi/2}\int_0^1\rho^2\sin\theta\,\mathrm{d}\rho\,\mathrm{d}\theta\,\mathrm{d}\varphi\right.$$
$$+2\beta\sum_{i=1}^{\infty}\sum_{j=1}^{\infty}\sum_{m=0}^{\infty}\sum_{n=1}^{\infty}A_{ij}B_{mn}X_i(\xi_0)Y_j(\eta_0)\int_0^{2\pi}\int_0^{\pi/2}\int_0^1\left\{\lambda_{mn}\rho^{\lambda_{mn}-1}P^m_{\lambda_{mn}}(\cos\theta)\cos m\varphi\right.$$
$$\left.\left.+\frac{1}{\rho}\rho^{\lambda_{mn}}\left\{\frac{\mathrm{d}P^m_{\lambda_{mn}}(\cos\theta)}{\mathrm{d}\theta}\right\}\cos m\varphi-\frac{m}{\rho\sin\theta}\rho^{\lambda_{mn}}P^m_{\lambda_{mn}}(\cos\theta)\sin m\varphi\right\}\rho^2\sin\theta\,\mathrm{d}\rho\,\mathrm{d}\theta\,\mathrm{d}\varphi\right]$$
$$+\bar{\Omega}^2\omega^2\sum_{m=0}^{\infty}\sum_{n=1}^{\infty}\sum_{q=0}^{\infty}\sum_{s=1}^{\infty}B_{mn}B_{qs}\int_0^{2\pi}\int_0^{\pi/2}\left\{\lambda_{qs}P^m_{\lambda_{mn}}(\cos\theta)P^q_{\lambda_{qs}}(\cos\theta)\cos m\varphi\cos q\varphi\right\}\sin\theta\,\mathrm{d}\theta\,\mathrm{d}\varphi$$
$$-2\int_0^{2\pi}\int_0^{\pi/2}\left[-\sum_{m=0}^{\infty}\sum_{n=1}^{\infty}\sum_{q=0}^{\infty}\sum_{s=1}^{\infty}B_{mn}B_{qs}\lambda_{mn}\lambda_{qs}P^m_{\lambda_{mn}}(\cos\theta)P^q_{\lambda_{qs}}(\cos\theta)\cos m\varphi\cos q\varphi\right.$$
$$+\frac{1}{2}\sum_{m=0}^{\infty}\sum_{n=1}^{\infty}\sum_{q=0}^{\infty}\sum_{s=1}^{\infty}B_{mn}B_{qs}\lambda_{mn}\lambda_{qs}\left\{\frac{\mathrm{d}P^m_{\lambda_{mn}}(\cos\theta)}{\mathrm{d}\theta}\right\}\left\{\frac{\mathrm{d}P^q_{\lambda_{qs}}(\cos\theta)}{\mathrm{d}\theta}\right\}\cos m\varphi\cos q\varphi$$
$$\left.+\frac{1}{2\sin^2\theta}\sum_{m=0}^{\infty}\sum_{n=1}^{\infty}\sum_{q=0}^{\infty}\sum_{s=1}^{\infty}B_{mn}B_{qs}mq\lambda_{mn}\lambda_{qs}P^m_{\lambda_{mn}}(\cos\theta)P^q_{\lambda_{qs}}(\cos\theta)\sin m\varphi\sin q\varphi\right]\sin\theta\mathrm{d}\theta\,\mathrm{d}\varphi. \tag{46}$$

In the above equation, we shall use integration formula on the trigonometric functions $\sin m\varphi$ and $\cos m\varphi$, and on the associated *Legendre* function $P^m_{\lambda_{mn}}(\cos\theta)$ as Eq. (18), (19) and

$$\int_0^{\pi/2}P_{\lambda_{0n}}(\cos\theta)\sin\theta\,\mathrm{d}\theta=\begin{cases}1\quad\text{for } s=0;\quad 0\quad\text{for } s>0: & \lambda_{0n}=2s,\\ \dfrac{P_{2s}(o)}{2s+2}=\dfrac{(-1)^s(2s-1)!}{(2s+2)!}: & \lambda_{0n}=2s+1,\end{cases} \tag{47}$$

$$M_{0n}=\int_0^{\frac{\pi}{2}}\left\{\frac{\partial P_{\lambda_{0n}}(\cos\theta)}{\partial\theta}\right\}\sin\theta\,\mathrm{d}\theta. \tag{48}$$

Finally, we obtain

$$\tilde{\tilde{L}}=\bar{\Delta}\omega^2\sum_{i=1}^{\infty}\sum_{j=1}^{\infty}A_{ij}^2\delta_{ik}\delta_{jl}-\bar{\Delta}\sum_{i=1}^{\infty}\sum_{j=1}^{\infty}\sum_{k=1}^{\infty}\sum_{l=1}^{\infty}A_{ij}A_{kl}[(\alpha_i^4+\lambda^4\beta_j^4)\delta_{ik}\delta_{jl}$$
$$+\nu\lambda^2(J^{20}_{ik}K^{02}_{jl}+J^{02}_{ik}K^{20}_{jl})+2(1-\nu)\lambda^2J^{11}_{ik}K^{11}_{jl}]$$
$$+2\pi\bar{\Omega}^2\omega^2\left[\frac{\beta^2}{3}\sum_{i=1}^{\infty}\sum_{j=1}^{\infty}\sum_{k=1}^{\infty}\sum_{l=1}^{\infty}A_{ij}A_{kl}X_i(\xi_0)X_k(\xi_0)Y_j(\eta_0)Y_l(\eta_0)\right.$$
$$\left.+2\beta\sum_{i=1}^{\infty}\sum_{j=1}^{\infty}\sum_{n=1}^{\infty}A_{ij}B_{0n}X_i(\xi_0)Y_j(\eta_0)\frac{M_{0n}}{\lambda_{0n}+2}\right]$$
$$+\frac{\pi\bar{\Omega}^2\omega^2}{2}\sum_{n=1}^{\infty}B_{0n}^2\frac{\lambda_{0n}}{2\lambda_{0n}+1}-\pi\sum_{n=1}^{\infty}B_{0n}^2\lambda_{0n}^2\left\{-\frac{1}{2\lambda_{0n}+1}+\frac{\lambda_{0n}(\lambda_{0n}+1)}{2(2\lambda_{0n}+1)}\right\},$$
$$i=1,2,\ldots,\quad j=1,2,\ldots,\quad k=1,2,\ldots,i,\quad l=1,2,\ldots,j,\quad n=1,2,\ldots. \tag{49}$$

It should be noted here that from the orthogonality of the trigonometric functions, only $m = q = 0$ terms, i.e. λ_{0n}, have been remained in the integration of summation terms in m and q in Eq. (46), where λ_{0n} corresponds to λ_{mn} when $m = 0$ and are even integers, i.e. 2, 4, 6, …. Integrations for the beam functions $X_i(\xi)$ and $Y_j(\eta)$, J_{ik}^{11}, K_{jl}^{11}, etc. shown above are presented in Appendix A.

Applying *Rayleigh–Ritz* method to the above equation

$$\frac{\partial \tilde{\tilde{L}}}{\partial A_{ij}} = 0, \quad \frac{\partial \tilde{\tilde{L}}}{\partial B_{0n}} = 0, \tag{50}$$

$$\begin{aligned}\frac{\partial \tilde{\tilde{L}}}{\partial A_{ij}} &= 2\bar{\Delta}\omega^2 \sum_{k=1}^{\infty}\sum_{l=1}^{\infty} A_{kl}\delta_{ik}\delta_{jl} \\ &\quad - 2\bar{\Delta}\sum_{k=1}^{\infty}\sum_{l=1}^{\infty} A_{kl}\left[(\alpha_i^4 + \lambda^4\beta_j^4)\delta_{ik}\delta_{jl} + \nu\lambda^2(J_{ik}^{20}K_{jl}^{02} + J_{ik}^{02}K_{jl}^{20}) + 2(1-\nu)\lambda^2 J_{ik}^{11}K_{jl}^{11}\right] \\ &\quad + 4\pi\bar{\Omega}^2\omega^2\left[\frac{\beta^2}{3}\sum_{k=1}^{\infty}\sum_{l=1}^{\infty} A_{kl}X_i(\xi_0)X_k(\xi_0)Y_j(\eta_0)Y_l(\eta_0) + \beta\sum_{n=1}^{\infty} B_{0n}X_i(\xi_0)Y_j(\eta_0)\frac{M_{0n}}{\lambda_{0n}+2}\right] = 0,\end{aligned} \tag{51}$$

$$\begin{aligned}\frac{\partial \tilde{\tilde{L}}}{\partial B_{0n}} &= 4\pi\beta\bar{\Omega}^2\omega^2\sum_{i=1}^{\infty}\sum_{j=1}^{\infty} A_{ij}X_i(\xi_0)Y_j(\eta_0)\frac{1}{\lambda_{0n}+2}M_{0n} \\ &\quad + \pi B_{0n}\left\{\bar{\Omega}^2\omega^2 - \lambda_{0n}(\lambda_{0n}-1)(\lambda_{0n}+2)\right\}\frac{\lambda_{0n}\delta_{ns}}{2\lambda_{0n}+1} = 0.\end{aligned} \tag{52}$$

Then we can obtain frequency equation in the matrix form as

$$\left[\begin{bmatrix}\bar{\Delta}K_{ijkl} & 0 \\ 0 & \dfrac{\pi\lambda_{0n}^2(\lambda_{0n}-1)(\lambda_{0n}+2)\delta_{ns}}{2\lambda_{0n}+1}\end{bmatrix} - \omega^2\begin{bmatrix}2\left\{\bar{\Delta}\delta_{ik}\delta_{jl} + \dfrac{2\pi\beta^2\bar{\Omega}^2}{3}X_i(\xi_0)X_k(\xi_0)Y_j(\eta_0)Y_l(\eta_0)\right\} & 4\pi\beta\bar{\Omega}^2X_i(\xi_0)Y_j(\eta_0)\dfrac{M_{0n}}{\lambda_{0n}+2} \\ 4\pi\beta\bar{\Omega}^2X_i(\xi_0)Y_j(\eta_0)\dfrac{M_{0n}}{\lambda_{0n}+2} & \dfrac{\pi\bar{\Omega}^2\lambda_{0n}\delta_{ns}}{2\lambda_{0n}+1}\end{bmatrix}\right]\begin{Bmatrix}A_{kl} \\ B_{0n}\end{Bmatrix} = \mathbf{0}, \tag{53}$$

where

$$K_{ijkl} = 2\left\{\left(\alpha_i^4 + \lambda^4\beta_j^4\right)\delta_{ik}\delta_{jl} + \nu\lambda^2\left(J_{ik}^{20}K_{jl}^{02} + J_{ik}^{02}K_{jl}^{20}\right) + 2(1-\nu)\lambda^2 J_{ik}^{11}K_{jl}^{11}\right\} \tag{54}$$

or putting

$$\mathbf{M} = \begin{bmatrix}2\left\{\bar{\Delta}\delta_{ik}\delta_{jl} + \dfrac{2\pi\beta^2\bar{\Omega}^2}{3}X_i(\xi_0)X_k(\xi_0)Y_j(\eta_0)Y_l(\eta_0)\right\} & 4\pi\beta\bar{\Omega}^2X_i(\xi_0)Y_j(\eta_0)\dfrac{M_{0n}}{\lambda_{0n}+2} \\ 4\pi\beta\bar{\Omega}X_i(\xi_0)Y_j(\eta_0)\dfrac{M_{0n}}{\lambda_{0n}+2} & \dfrac{\pi\bar{\Omega}^2\lambda_{0n}\delta_{ns}}{(2\lambda_{0n}+1)}\end{bmatrix}, \tag{55}$$

$$\mathbf{K} = \begin{bmatrix}\bar{\Delta}K_{ijkl} & 0 \\ 0 & \dfrac{\pi\lambda_{0n}^2(\lambda_{0n}-1)(\lambda_{0n}+2)\delta_{ns}}{2\lambda_{0n}+1}\end{bmatrix}, \tag{56}$$

Eq. (53) yields

$$\left[\mathbf{K}-\omega^2\mathbf{M}\right]\left\{\begin{array}{c}A_{ij}\\B_{0n}\end{array}\right\}=\mathbf{0} \tag{57}$$

from which one can obtain coupled natural frequencies as eigenvalues, and vibration modes as eigenvectors.

3.3. Numerical results

The present plate–drop coupled dynamical system can be represented by six system parameters: aspect ratio of the plate $\lambda \equiv L/H$, plate thickness ratio $\alpha \equiv h/L$, drop radius ratio $\beta = h/a$, density ratio $\bar{\rho} \equiv \rho_p/\rho_d$, surface tension parameter $\delta \equiv \sigma h^2/D$, and attached position of the drop (ξ_0, η_0). Numerical calculations have been carried out varying these system parameters to clarify the influence of attached drop on the coupled dynamical characteristics of a plate. Poisson's ratio ν was taken as 0.3. In the calculation, unknown terms in Eq. (53) were taken up to $i=j=k=l=n\ =8$, to obtain reliable values as engineering data. Numerical calculations have been conducted programming ourselves by FORTRAN except subroutine programs, which find eigenvalue and eigenvector and are developed as Library program of Computer Center of Tohoku University, Japan.

3.3.1. Uncoupled vibrations of plate and drop

First of all, we shall see the uncoupled vibration characteristics of a plate alone. Variations of uncoupled natural frequencies of a cantilever plate ω_p with aspect ratioλ are shown in Fig. 4. In the numerical calculation,

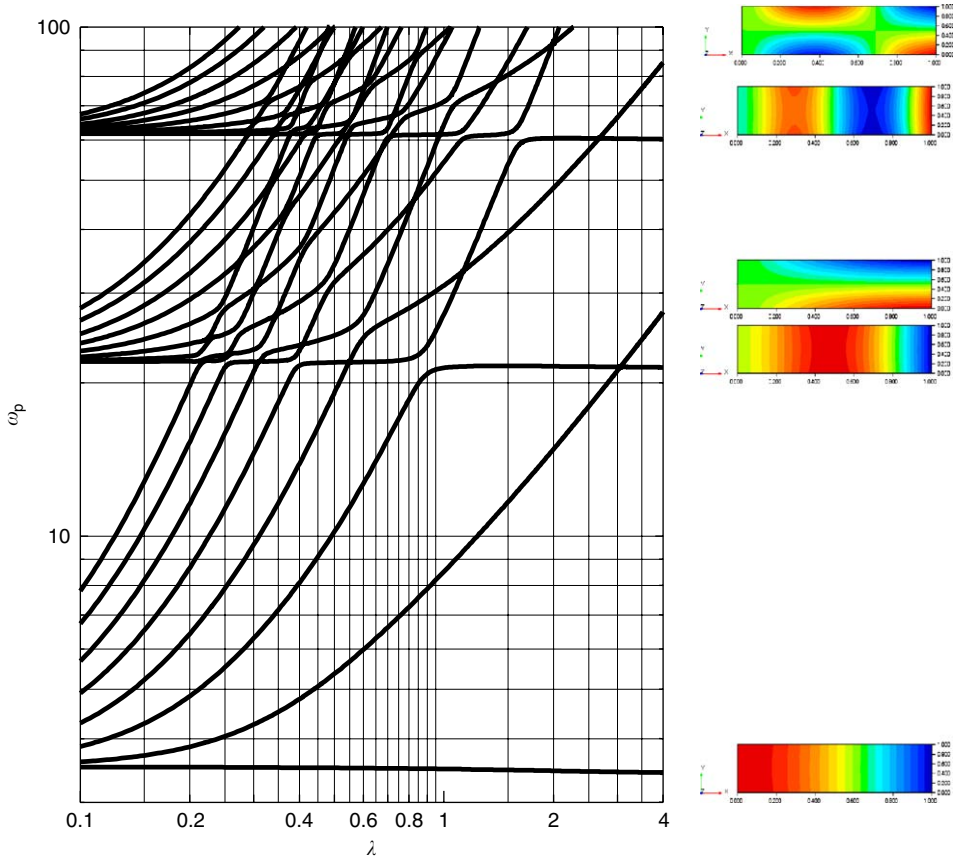

Fig. 4. Variation of natural frequency of a cantilever plate ω_p with aspect ratio λ.

unknown terms were taken as $k = 8$, $l = 8$. For convenience, vibration modes when $\lambda = 4.0$ are presented in the right-hand side of the figure. In general, natural frequencies that have nodal line in vibration mode perpendicular to the plate axis (ξ) are nearly constant with λ, while those, which have nodal line parallel to the plate axis, increase with increase in λ. With the variation of λ, exchange of the vibration modes can be observed. Furthermore, one can recognize the veering and crossing of the frequency curves [26,27]. In order to distinguish these two, step size for λ in the numerical calculation was taken to be small as much as possible. More details on frequency curve's veering and crossing in a cantilever plate have been studied in Ref. [25]. The lowest four vibration modes are presented for three kinds of the aspect ratio $\lambda = 0.5$, 1 and 2 in Fig. 5.

While uncoupled natural frequency of a drop ω_d can be obtained by putting $A_{kl} \equiv 0$ in Eq. (53), or a non-dimensional form of Eq. (24),

$$\omega_d = \frac{1}{\bar{\Omega}} \sqrt{\lambda_{0n}(\lambda_{0n} - 1)(\lambda_{0n} + 2)}, \tag{58}$$

where $\lambda_{0n} = 2, 4, \ldots$. Corresponding vibration modes are axisymmetric with $m = 0$, as described in Section 3.2. Variations of the natural frequency ω_d with radius ratio β and density ratio $\bar{\rho}$ are presented in Figs. 6 and 7, respectively, for three values of surface tension parameter δ, 1.0×10^{-7}, 1.0×10^{-6}, 1.0×10^{-5} for $\alpha = 0.01$. From these figures, we find that natural frequencies drastically increase with increase in the surface tension parameter δ.

3.3.2. *Plate-drop coupled system*

As already mentioned, since the present coupled dynamical system includes six system parameters, i.e. λ, α, β, $\bar{\rho}$, δ and (ξ_0, η_0), it may be impossible to show all the cases in the combination of theses parameters. Then,

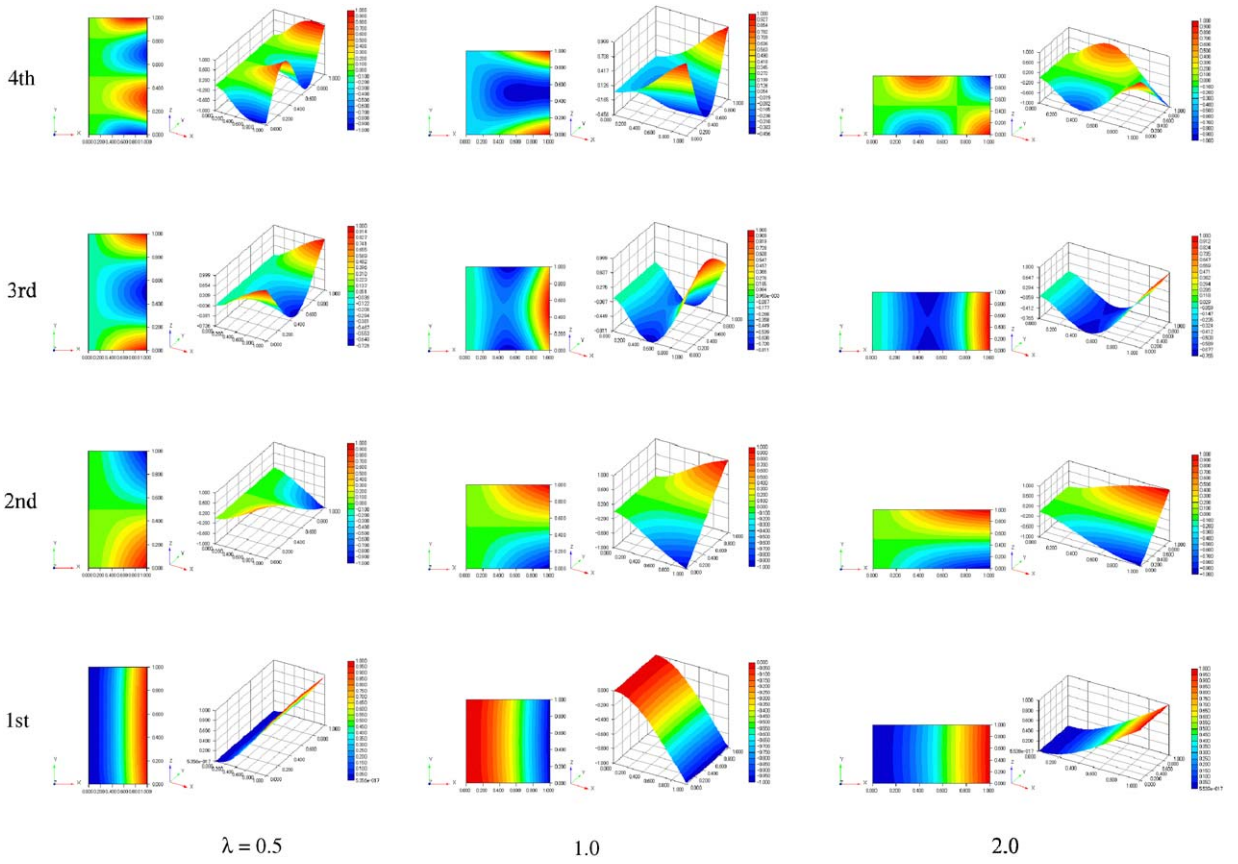

Fig. 5. Vibration modes of a cantilever plate with aspect ratio λ.

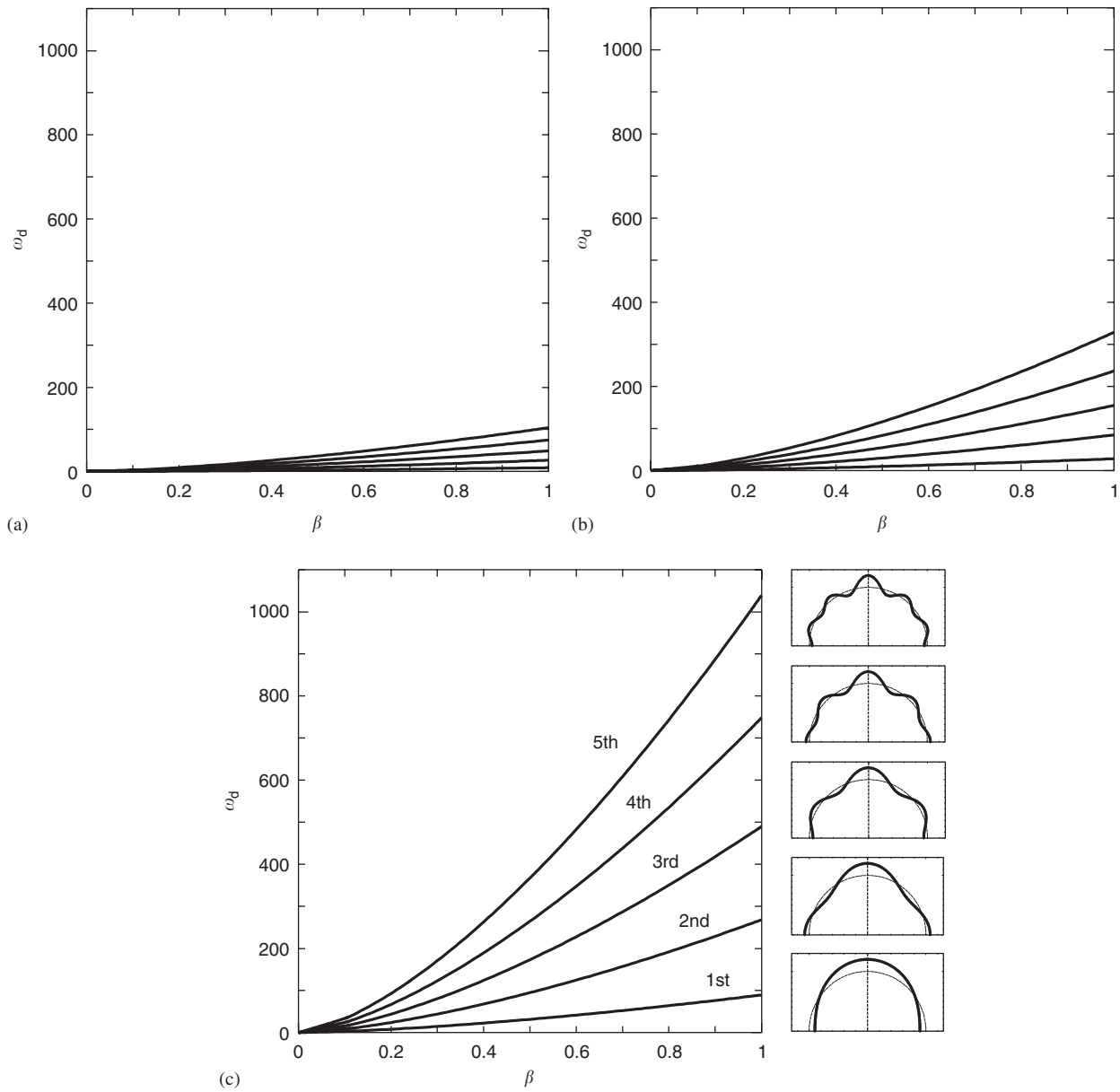

Fig. 6. Axisymmetric natural frequency of a semi-spherical drop ω_d with drop radius ratio β, $\alpha = 0.01$; (a) $\delta = 1.0 \times 10^{-7}$; (b) $\delta = 1.0 \times 10^{-6}$; (c) $\delta = 1.0 \times 10^{-5}$.

we would like to concentrate here to demonstrate the coupling between one multi-degree of freedom system, i.e. a cantilever plate, and added another multi-degree of freedom system, i.e. a liquid drop, and to compare the results with the coupled system between one multi-degree of freedom system, i.e. a cantilever plate, and single-degree of freedom system, i.e. 'mass–spring' system which has been previously studied [6]. Therefore, for instance, we set here the aspect ratio of the plate $\lambda = 1.0$, position of the liquid drop $(\xi_0, \eta_0) = (0.5, 0.5)$.

Coupled natural frequency variations with density ratio $\bar{\rho}$ are presented for three values of surface tension parameter δ in Fig. 8, when $\beta = 0.5$, $\alpha = 0.01$. In the figure, although uncoupled natural frequencies of the drop ω_d and those of the plate ω_p are presented in one-dotted curves or broken lines, they are almost under coupled frequency curves which are presented with thick solid lines or curves. Horizontal lines are coupled plate natural frequencies, which are independent with $\bar{\rho}$, and parabolic curves are coupled drop natural

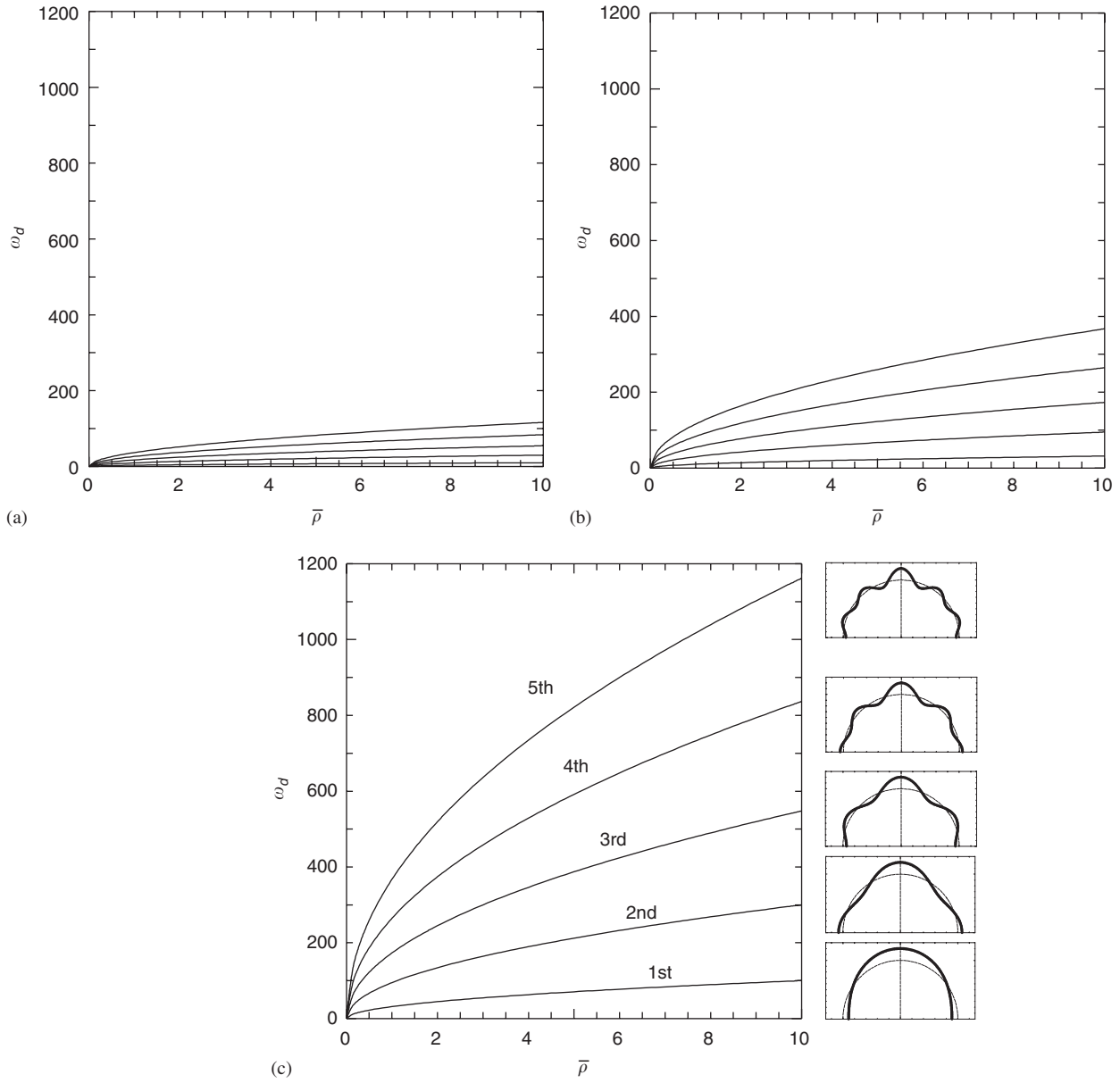

Fig. 7. Axisymmetric natural frequency of a semi-spherical drop ω_d with density ratio $\bar{\rho}$, $\alpha = 0.01$; (a) $\delta = 1.0 \times 10^{-7}$; (b) $\delta = 1.0 \times 10^{-6}$; (c) $\delta = 1.0 \times 10^{-5}$.

frequencies. In the case when surface tension is moderately large with $\delta = 1.0 \times 10^{-5}$ shown in Fig. 8(a), crossings between parabolic curves and horizontal lines can be seen just at the small value region of $\bar{\rho}$ near the ordinate. However, as shown in Fig. 7, in which uncoupled natural frequency variations of drop with $\bar{\rho}$, with decrease in δ the coupled natural frequencies of the drop decrease and the number of cross-points with horizontal lines gradually increases (Fig. 8(b) and (c)). In these crossing regions, the coupling may be significant between drop motion and plate motion.

Variation of the lowest four coupled vibration modes are presented in Fig. 9, when $\delta = 1.0 \times 10^{-7}$ which corresponds to Fig. 8(c), for $\bar{\rho} = 1, 5, 10$. We see that the order of vibration modes changes with $\bar{\rho}$, i.e. modes in which liquid drop deformation is predominant and those in which plate motion is predominant.

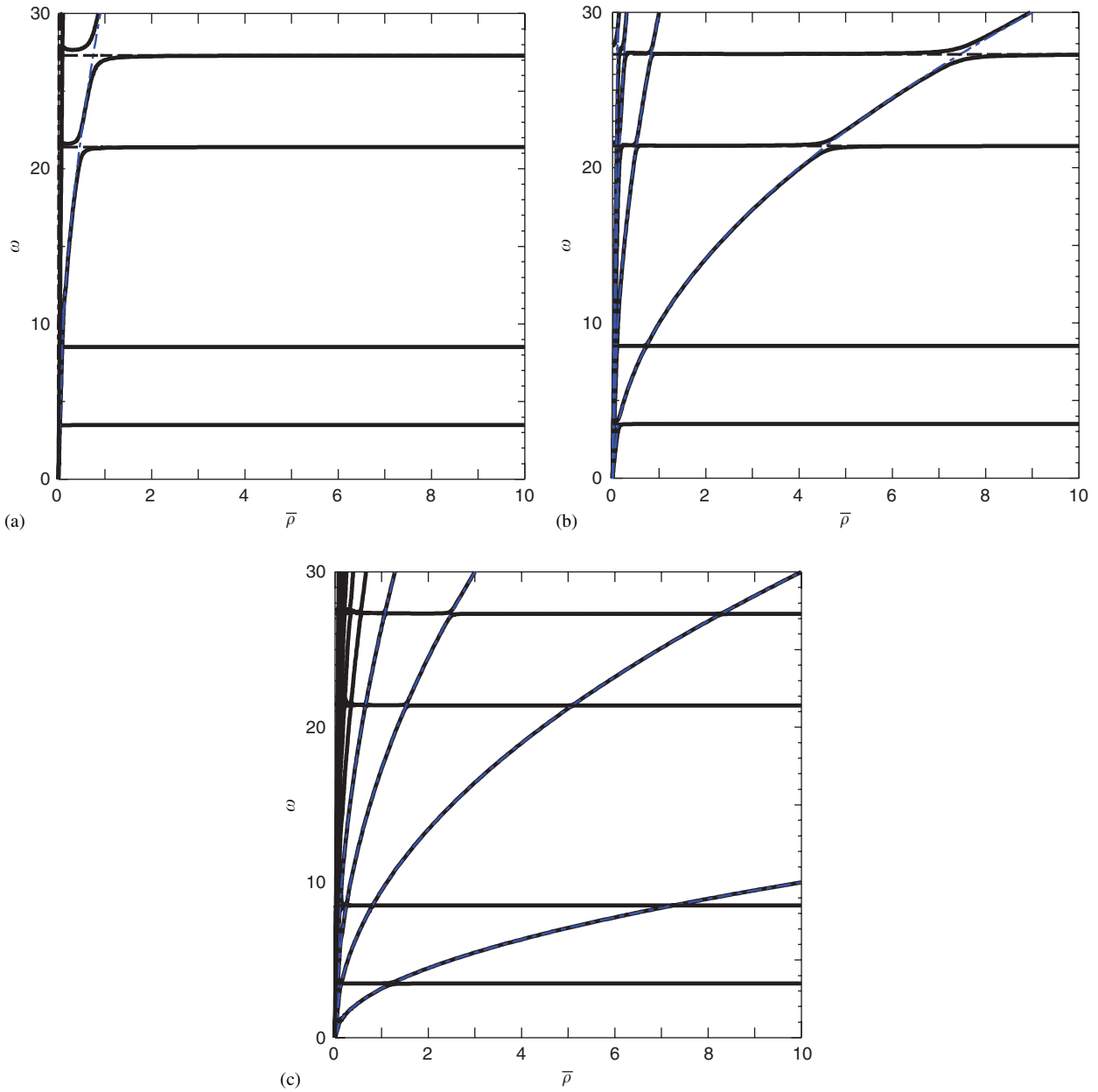

Fig. 8. Coupled natural frequencies ω with density ratio $\bar{\rho}$, $(\xi_0, \eta_0) = (0.5, 0.5)$, $\beta = 0.5$, $\alpha = 0.01$: (a) $\delta = 1.0 \times 10^{-5}$; (b) $\delta = 1.0 \times 10^{-6}$; (c) $\delta = 1.0 \times 10^{-7}$.

Finally, we shall compare the dynamical coupling characteristics of the present system with those of a plate carrying a 'spring–mass' system [6]. In the previous study [6], we have analyzed coupled vibration characteristics of a cantilever plate with attached 'spring–mass' system, i.e. the liquid drop was simply modeled as a 'spring–mass' system.

Fig. 10(a) shows $\omega - \alpha_{m_e}$ diagram of the previous system [6] when 'spring–mass' system is attached on the center of a cantilever plate $(\xi_0,\ \eta_0) = (0.5,\ 0.5)$, where α_{m_e} is the mass ratio $(\equiv m_e/\rho HhL)$, when stiffness parameter $\alpha_{ke} \equiv k_e L^2/D = 10$, plate thickness ratio $\alpha \equiv h/L = 0.01$, aspect ratio $\lambda = 1.0$. In the figure, horizontal one-dotted lines are uncoupled natural frequencies of the plate, while a red broken curve corresponds to that of 'spring–mass' system. We found that with increasing α_{m_e}, e.g. increasing mass m_e,

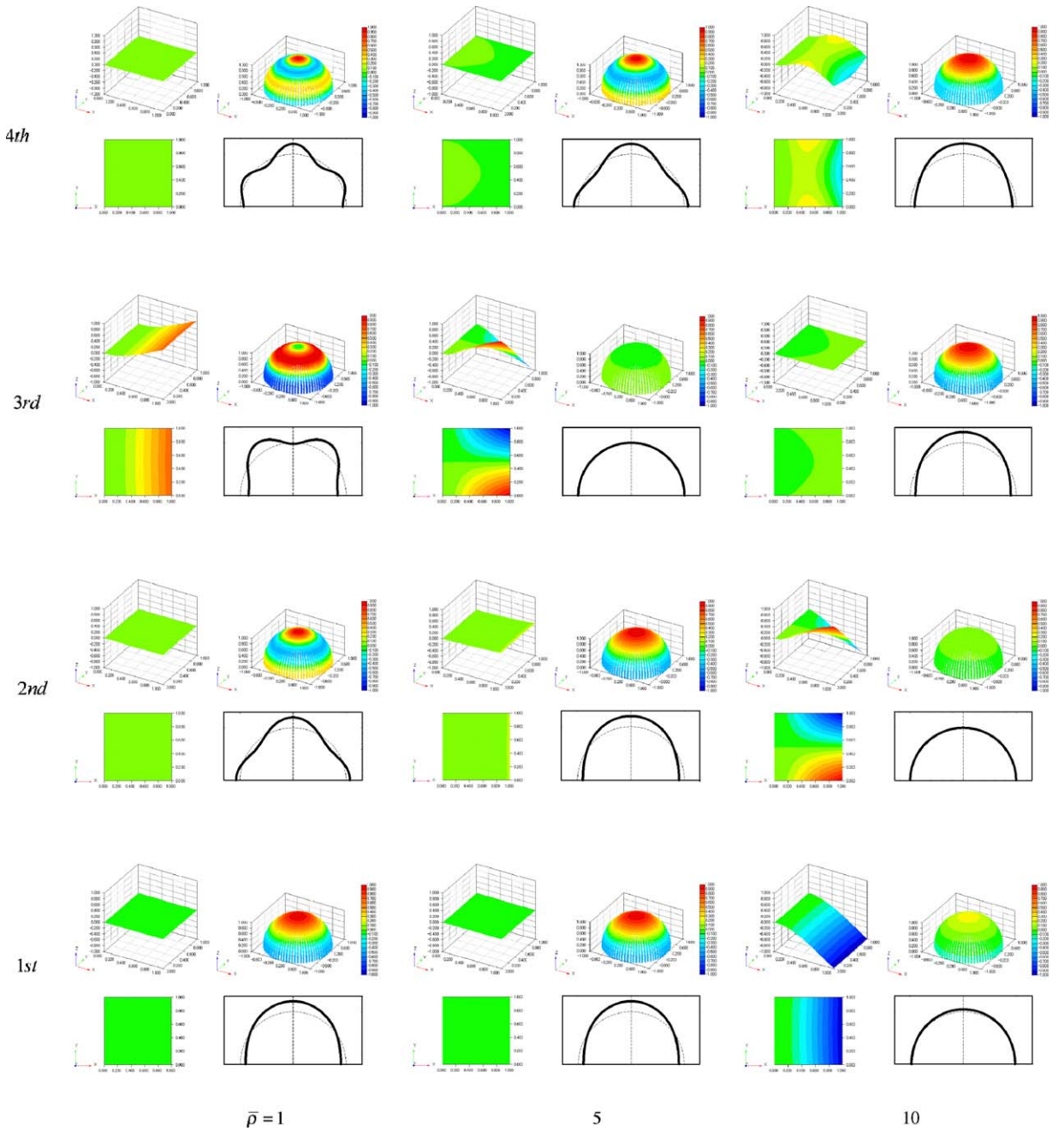

Fig. 9. Coupled vibration modes with density ratio $\bar{\rho}$, $(\xi_0, \eta_0) = (0.5, 0.5)$, $\beta = 0.5$, $\alpha = 0.01$, $\delta = 1.0 \times 10^{-7}$.

uncoupled natural frequency of 'spring–mass' system decreases, and that at the regions crossing points between one-dotted lines and a red curve, there seems curve veering in coupled natural frequency curves (shown in broken lines), and an exchange of vibration modes can be recognized.

While for the present case in which plate and a liquid drop are coupling, we choose, for example, reciprocal of β, $1/\beta = a/h$, as a variable parameter in the abscissa, then we get similar $\omega - 1/\beta$ diagram shown in Fig. 10(b). In the figure, the lowest five coupled natural frequency curves are mainly presented together with uncoupled natural frequencies of the plate and the drop with horizontal broken lines and one-dotted curves, respectively. Other system parameters are taken as $\bar{\rho} \equiv \rho_p/\rho_d = 0.5$, $\delta = 1.0 \times 10^{-6}$,

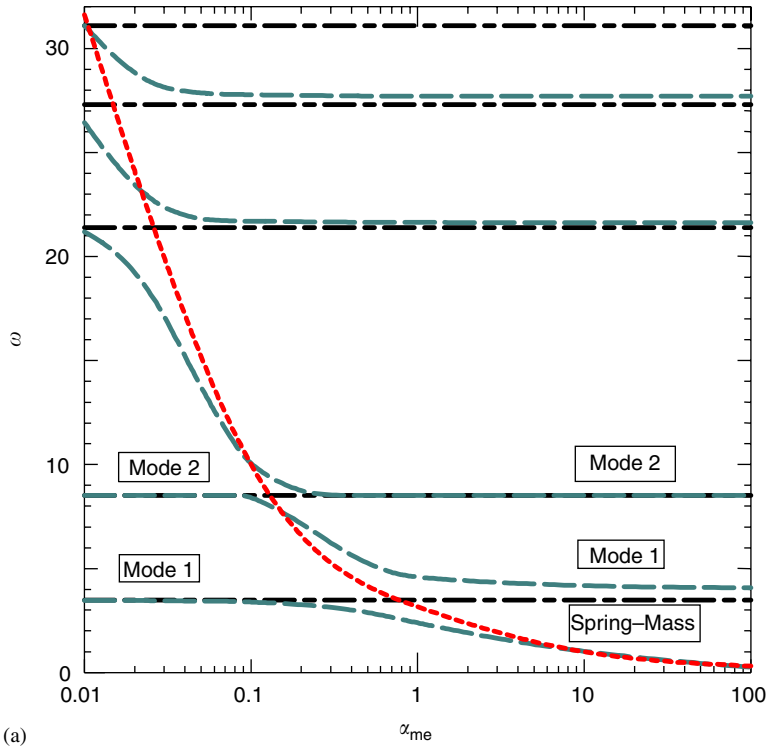

(a)

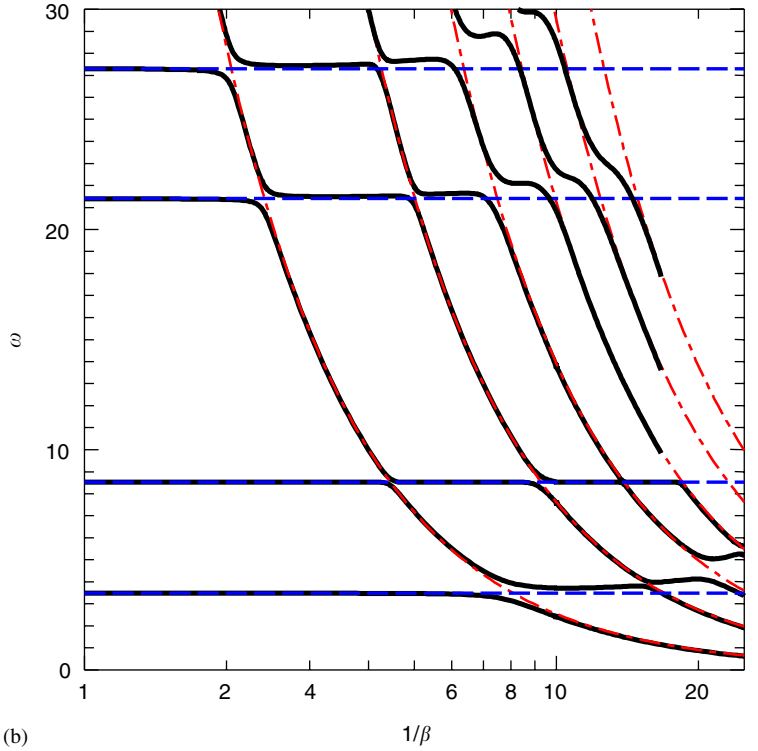

(b)

Fig. 10. Comparison of coupled natural frequency ω variations, $\lambda = 1.0, (\xi_0, \eta_0) = (0.5, 0.5)$; (a) 'spring–mass' system, $\alpha = 0.01$ [6]; (b) present case, $\beta = 0.5$, $\alpha = 0.005$, $\bar{\rho} = 0.5, \delta = 1.0 \times 10^{-6}$.

$\alpha \equiv h/L = 0.005$, $(\xi_0, \eta_0) = (0.5, 0.5)$. First, we shall follow the lowest frequency curve along the abscissa $1/\beta$, it is nearly straight line until $1/\beta \approx 8$ and corresponds to a coupled natural frequency in which plate motion is predominant. At $1/\beta \approx 8$ region, this line makes curve veering with coupled drop frequency curve which rapidly downs from the upper-left side in the diagram, i.e. this line turns down following the uncoupled drop frequency, and coupled drop frequency curve follows the horizontal line. At this region, an exchange of vibration modes occurs, i.e. former downward frequency curve tends to that for the coupled drop frequency, while the latter horizontal frequency line tends to that for the coupled plate frequency, respectively. Further increase in $1/\beta$, the horizontal line made the second veering with coupled drop frequency curve of the 2nd mode. Similar curve veerings continue infinitely because the added liquid drop has infinite number of freedom, i.e. infinite number of vibration modes. This is a significant different characteristic of the present system from the previous case with coupled 'spring–mass' system [6].

The same is true for the higher vibration mode curves of a coupled plate frequency. Note that similar diagram can be obtained by choosing $1/\bar{\rho} \equiv \rho_d/\rho_p$ as a variable parameter in the abscissa.

4. Conclusions

From the energy point of view, by using *Rayleigh–Ritz* method, we have formulated the coupled free vibration problems between a cantilever thin elastic plate and a hemi-spherical liquid drop attached on in zero-gravity condition, which finally rendered into an eigenvalue problem. In some numerical calculations, difference of the vibrational characteristics of the present coupled system in which plate and liquid drop are coupling, i.e. one multi-degree of freedom system and another multi-degree of freedom system are coupling, and those of the previous one [6] in which plate and a 'spring–mass' system are coupling, i.e. multi-degree of freedom system and a single-degree of freedom system are coupling, have been demonstrated.

Appendix A. Integration shown in Eq. (63)

Integration involving clamped–free beam function $X_i(\xi)$:

$$J_{ik}^{00} \equiv \int_0^1 X_i(\xi) X_k(\xi)\,\mathrm{d}\xi = \delta_{ik}, \tag{A.1}$$

$$J_{ik}^{11} \equiv \int_0^1 \frac{\partial X_i(\xi)}{\partial \xi}\frac{\partial X_k(\xi)}{\partial \xi}\,\mathrm{d}\xi = \begin{cases} (3+\alpha_i Q_i)\alpha_i Q_i - \alpha_i \nu_i \mu_i & (i=k), \\ 4(C_{ik}-C_{ki})/(\alpha_i^4 - \alpha_k^4) & (i \neq k), \end{cases} \tag{A.2}$$

$$J_{ik}^{20} \equiv \int_0^1 \frac{\partial^2 X_i(\xi)}{\partial \xi^2} X_k(\xi)\,\mathrm{d}\xi = \begin{cases} (1-\alpha_i Q_i)\alpha_i Q_i + \alpha_i \nu_i \mu_i & (i=k), \\ 4\alpha_i Q_i - 4(C_{ik}-C_{ki})/(\alpha_i^4 - \alpha_k^4) & (i \neq k), \end{cases} \tag{A.3}$$

$$J_{ik}^{22} \equiv \int_0^1 \frac{\partial^2 X_i(\xi)}{\partial \xi^2}\frac{\partial^2 X_k(\xi)}{\partial \xi^2}\,\mathrm{d}\xi = \alpha_i^4 \delta_{ik}, \tag{A.4}$$

$$C_{ik} = \alpha_i^3 \alpha_k (\alpha_i \cdot Q_k - \nu_i \cdot \alpha_k \cdot \mu_k), \tag{A.5}$$

$$Q_i = \coth\,\alpha_i + \cot\,\alpha_i, \tag{A.6}$$

where δ_{ik} is Kronecker's delta.

Integration involving free–free beam function $Y_j(\eta)$:

$$K_{jl}^{00} \equiv \int_0^1 Y_j(\eta) Y_l(\eta)\,\mathrm{d}\eta = \delta_{jl}, \tag{A.7}$$

$$K_{jl}^{11} \equiv \int_0^1 \frac{\partial Y_j(\eta)}{\partial \eta} \frac{\partial Y_l(\eta)}{\partial \eta} \, \mathrm{d}\eta = \begin{cases} \beta_j \left\{ 3(\bar{Q}_j + \bar{\mu}_j \cdot \bar{\nu}_l) + \beta_j \bar{Q}_j^2 \right\} & (j = l), \\ 4(D_{jl} - D_{lj})/(\beta_j^4 - \beta_l^4) & (j \neq l), \end{cases} \tag{A.8}$$

$$K_{jl}^{20} \equiv \int_0^1 \frac{\partial^2 Y_j(\eta)}{\partial \eta^2} Y_l(\eta) \, \mathrm{d}\eta = \begin{cases} \beta_j(\bar{Q}_j + \bar{\mu}_j \cdot \bar{\nu}_j - \beta_j \cdot \bar{Q}_j^2) & (j = l), \\ 4\beta_j(\bar{Q}_j + \bar{\nu}_j \cdot \bar{\mu}_j) - 4(D_{jl} - D_{lj})/(\beta_j^4 - \beta_l^4) & (j \neq l), \end{cases} \tag{A.9}$$

$$K_{jl}^{22} \equiv \int_0^1 \frac{\partial^2 Y_j(\eta)}{\partial \eta^2} \frac{\partial^2 Y_l(\eta)}{\partial \eta^2} \, \mathrm{d}\eta = \beta_j^4 \delta_{jl}, \tag{A.10}$$

$$D_{jl} = \beta_j^4 \beta_l (\bar{Q}_l + \bar{\mu}_j \cdot \bar{\nu}_l), \tag{A.11}$$

$$\bar{Q}_j = \coth \beta_j + \cot \beta_j. \tag{A.12}$$

References

[1] H.U. Walter (Ed.), *Fluid Sciences and Materials Science in Space: A European Perspective*, Springer, Berlin, 1987.

[2] E.H. Trinh, J. Depew, Solid surface wetting and the deployment of drop in microgravity, *Microgravity Science and Technology* 7 (4) (1995) 299–306.

[3] I. Egry, D.A. Diefenbach, W. Dreier, J. Piller, Containerless processing in space-thermophysical property measurement using electromagnetic levitation, *Journal of Thermophysics* 22 (2001) 569–578.

[4] J.C. Legros, O. Dupont, P. Queeckers, S. van Vaerenbergh, D. Schwabe, Thermohydrodynamic instabilities and capillary flows, *Progress in Astronautics and Aeronautics* 130 (1990) 207–239.

[5] B.V. Tryggvason, R.F. Redden, R.A. Herring, W.M.B. Duval, R.W. Smith, K.S. Rezkallah, S. Varma, The vibration environment on the international space station: its significance to fluid-based experiments, *Acta Astronautica* 48 (2001) 59–70.

[6] M. Chiba, T. Sugimoto, Vibration characteristics of a cantilever plate with plate with attached spring–mass system, *Journal of Sound and Vibration* 260 (2) (2003) 237–263.

[7] J.W. Miles, On the sloshing of liquid in a flexible tank, *Journal of Applied Mechanics—Transactions of ASME* 25 (2) (1958) 277–283.

[8] J.C. Luke, A variational principle for a fluid with a free surface, *Journal of Fluid Mechanics* 27 (1967) 395–397.

[9] G.B. Whitham, Non-linear dispersion of water wave, *Journal of Fluid Mechanics* 27 (1967) 399–412.

[10] K. Komatsu, Non-linear sloshing analysis of liquid in tanks with arbitrary geometries, *International Journal of Non-Linear Mechanics* 22 (3) (1987) 193–207.

[11] R. Natarajan, R.A. Brown, Quadratic resonance in the three-dimensional oscillations of inviscid drops with surface tension, *Physics of Fluids* 29 (9) (1986) 2788–2797.

[12] R. Natarajan, R.A. Brown, Third-order resonance effects and the nonlinear stability of drop oscillations, *Journal of Fluid Mechanics* 183 (1987) 95–121.

[13] H. Azuma, S. Yoshihara, Three-dimensional large-amplitude drop oscillations: experiments and theoretical analysis, *Journal of Fluid Mechanics* 393 (1999) 309–332.

[14] D. Young, Vibration of beam with concentrated mass, spring, and dashpot, *Journal of Applied Mechanics—Transactions of ASME* 70 (1948) 65–72.

[15] Y.C. Das, D.R. Navakatna, Vibrations of a rectangular plate with concentrated mass, spring, and dashpot, *Journal of Applied Mechanics—Transactions of ASME* 30 (1963) 31–36.

[16] J.C. Snowdon, Vibrations of simply supported rectangular and square plates to which lumped masses and dynamic vibration absorbers are attached, *Journal of Acoustical Society of America* 57 (3) (1975) 646–654.

[17] J.W. Nicholson, L.A. Bergman, Free vibration of combined dynamical systems, *Journal of Engineering Mechanics* 112 (1986) 1–13.

[18] J.W. Nicolson, L.A. Bergman, Vibration of damped plate-oscillator systems, *Journal of Engineering Mechanics* 112 (1) (1986) 14–30.

[19] D. Trentin, J.L. Guyader, Vibrations of a master plate with attached masses using modal sampling method, *Journal of Acoustical Society of America* 96 (1) (1994) 235–245.

[20] E.H. Dowell, D. Tang, The high-frequency response of a plate carrying a concentrated mass/spring system, *Journal of Sound and Vibration* 213 (5) (1998) 843–863.

[21] P.D. Cha, W.C. Wong, A novel approach to determine the frequency equations of combined dynamical systems, *Journal of Sound and Vibration* 219 (4) (1999) 689–706.

[22] K.-M. Won, Y.-S. Park, Optimal support position for a structure to maximize its fundamental natural frequency, *Journal of Sound and Vibration* 213 (5) (1998) 801–812.

[23] J.-J. Wu, Free vibration characteristics of a rectangular plate carrying multiple three-degree-of-freedom spring–mass system using equivalent mass method, *International Journal of Solids and Structures* 43 (2006) 727–746.
[24] L. Rayleigh, On the capillary phenomena of jets, *Proceeding of the Royal Society of London* 29 (1879) 71–97.
[25] M. Chiba, I. Yoshida, Free vibration of a rectangular plate-beam coupled system, *Journal of Sound and Vibration* 194 (1) (1996) 49–65.
[26] A.W. Leissa, On a curve veering aberration, *Journal of Applied Mathematics and Physics* 25 (1974) 99–111.
[27] N.C. Perkins, C.D. Mote Jr., Comments on curve veering in eigenvalue problem, *Journal of Sound and Vibration* 106 (3) (1986) 451–463.